MAPPING AND CHARACTERIZATION OF 18-5 AND 12-5, GENES WHICH POTENTIALLY LINK THE RHOA SIGNALING PATHWAY TO THE ECDYSONE RESPONSE IN DROSOPHILA EPITHELIAL MORPHOGENESIS

by

SAMUEL E. FOX
BS Oregon State University

A thesis submitted in partial fulfillment of the requirements
for the degree of Master of Science
in the Department of Biology
in the College of Sciences
at the University of Central Florida
Orlando, Florida

Summer Term
2006

ABSTRACT

Systemic steroid hormone and intracellular signaling pathways are known to act cooperatively during the development of vertebrate and invertebrate epithelia. However, the mechanism of this interaction is poorly understood. Morphogenesis of Drosophila leg imaginal disc epithelia is regulated both by the steroid hormone 20-hydroxyecdysone (ecdysone) and the RhoA GTPase signaling pathway. Recent evidence suggests that these pathways act cooperatively to control imaginal disc morphogenesis. Thus, leg imaginal disc morphogenesis is an excellent system in which to study the interaction of steroid hormone and intracellular signaling pathways. We have identified mutations in three genes, *12-5*, *18-5*, and *31-6*, with roles in the morphogenesis of leg epithelia. Of particular interest, these mutations interact genetically with each other, mutations in the RhoA signaling pathway, and the ecdysone regulated *Sb-sbd* (*Stubble*) transmembrane serine protease. This suggests that the *12-5*, *18-5*, and *31-6* gene products may link hormone and RhoA signaling responses. The goal of this research was to identify and characterize the *18-5* and *12-5* genes in order to discern the mechanistic relationship between the RhoA pathway and ecdysone hierarchy.

18-5 and *12-5* were precisely mapped to molecular locations within the *Drosophila* genome utilizing a P-element recombination mapping technique. This work narrowed the location of the *18-5* locus to within an interval of 112 kb within the *Drosophila* genome sequence. This interval contains 17 known and predicted genes. I also mapped the location of the *12-5* locus to a 2.6 Mb interval of the 2nd chromosome. Based on phenotypic analyses and the

site of the molecularly mapped interval, a candidate gene for the *18-5* mutation was identified. Sequence analysis of the candidate gene was inconclusive and requires further analysis. Genetic interaction assays indicate that the *18-5* gene product acts upstream or at the level of Rho kinase in the RhoA signaling pathway.

I would like to dedicate this thesis to my mother Carol and my father Ron, all my friends here at UCF (especially Rob, Todd, Juan, Paul, Jack, and Jill), my mentor Dr. von Kalm, and of course, most of all, my wife Erin. I love you Erin.

TABLE OF CONTENTS

LIST OF FIGURES vii

LIST OF TABLES ix

INTRODUCTION 1

Ecdysone and *Drosophila melanogaster* development 3

Drosophila leg morphogenesis 5

Regulation of leg epithelial cell shape changes 6

RhoA GTPase signaling in imaginal discs 7

Stubble serine protease and a proposed regulatory model 11

Genes involved in leg morphogenesis identified in a genetic screen 13

Aims of this thesis 15

MATERIALS AND METHODS 16

Drosophila crosses 16

Deficiency mapping of *18-5* and *12-5* 17

Molecular mapping of *18-5* and *12-5* 17

Molecular mapping of the *18-5* mutation: 17

Molecular mapping of the 12-5 mutation 20

18-5 suppression analysis 21

Sequencing of *DRal GEFmeso* 22

RESULTS 26

Preliminary genetic interaction data 26
Deficiency mapping of *18-5* 27
Molecular mapping of the *18-5* gene 31
Testing mutations and transgene insertions within the mapped region for complementation with *18-5* 36
18-5 genetic interactions 38
Sequencing of DRal GEFmeso in *18-5* homozygotes 42
Genetic interaction studies place *18-5* at or above Drok in the RhoA pathway 45
Deficiency mapping of *12-5* 48
Further mapping of the *12-5* locus 50
12-5 genetic interactions 51
DISCUSSION 54
Deficiency and recombination mapping of *18-5* 56
18-5 genetic interactions 58
GEFmeso 59
Possibility that *18-5* and *12-5* are alleles warrants additional analysis 61
Broader Significance 62
Future Directions 64
REFERENCES 67

LIST OF FIGURES

Figure 1: Changes in ecdysone titer at the onset of metamorphosis. 4

Figure 2: Illustration depicting the cell shape changes during leg elongation. 6

Figure 3: Image depicting the leg and wing wildtype (A and C) and malformed (B and D) phenotypes. 7

Figure 4: The Rho GTPase cycle. Rho GTPases are regulated by GEFs, GAPs and GDIs. 9

Figure 5: Model of RhoA mediated signaling in imaginal discs. 10

Figure 6: Structure of the *Drosophila* type II transmembrane serine protease. 11

Figure 7: Proposed mechanisms regulating the activation of RhoA in imaginal discs: 13

Figure 8: This schematic explains the crossing scheme used to conduct the P-element recombination mapping. 18

Figure 9: Strategy for distinguishing white eye F2 non-recombinants from the F2 recombinants. 20

Figure 10: Representative schematic of the suppression analysis crosses. 22

Figure 11: Image depicting the deficiency mapping of *18-5*. 28

Figure 12: Image depicting the P-element insertions used to further define the boundaries of the deficiency Df(2R)Pu66 used to map *18-5*. 30

Figure 13: Schematic depicting the P-element recombination mapping technique. 32

Figure 14: This figure shows the formula used to calculate the projected molecular position (PMP) of the *18-5* mutation. 34

Figure 15: Image depicting the P-elements (triangles with dashes indicating their respective positions) used to map the *18-5* gene and the deficiencies defining the smallest mapped region in which the *18-5* gene is located. 35
Figure 16: Genomic region in which *18-5* was mapped. 36
Figure 17: Wing malformation phenotype depicting the extra crossvein. 39
Figure 18: Schematic of GEFmeso structure [53] 42
Figure 19: Locations of primers used for the PCR amplification of GEFmeso. 43
Figure 20: Image showing the nine bp insertion in *GEFmeso* gene sequenced from *18-5* and *12-5* homozygotes (left). This insertion results in a three amino acid insertion of aspartic acid and two proline residues into the GEFmeso protein (right). 44
Figure 21: Model of RhoA mediated signaling in imaginal discs. 46
Figure 22: Schematic of the second chromosome and the P-elements used to map *12-5*. 51

LIST OF TABLES

Table 1: Primers used for the PCR amplification of *GEFmeso*. 23

Table 2: Thermocycler settings for the PCR amplification of *GEFmeso*. 24

Table 3: *18-5* and *12-5* genetic interactions with ecdysone activated Stubble and members of the RhoA signaling pathway regulating leg morphogenesis. 26

Table 4: This table indicates the results of the complementation tests conducted to more precisely define the right boundary of Df(2R)Pu66. 27

Table 5: Lethal P-element insertions used to better define the breakpoints of the deficiency, Df(2R)Pu66. 29

Table 6: *18-5/*P-element recombination data used to calculate the molecular position of the *18-5* locus. 33

Table 7: Results of complementation tests between *18-5* and various transgene insertions within or close to the 112 kb region containing the *18-5* locus. 37

Table 8: Genetic interactions of *18-5*. 41

Table 9: Suppression analysis of *18-5* malformation by cofilin phosphatase (*ssh*) and the myosin binding subunit of myosin phosphatase (Mbs^3). 47

Table 10: List of deficiencies and their locations which were complementation tested with *12-5*. 49

Table 11: Table showing the viability of trans-heterozygote animals involving *12-5* or *18-5*. 49

Table 12: Recombination distances between various P-elements and *12-5*. 50

Table 13: Genetic interactions of the *12-5* mutation. 53

INTRODUCTION

Epithelia are one of the four primary tissues and occur in various morphological types to provide a wide variety of functions. These functions include: secretion, absorption, and sensation detection as well as the more general structural, protective and partitioning functions. One of the most important characteristics of epithelia is that cells adhere to each other to form nearly impermeable, laterally coherent sheets. Several cell junction types mediate cell-cell interactions in epithelia (e.g. tight junctions, gap junctions and desmosomes). Adherens junctions are a type of cell junctions which provide lateral adhesion and tension between epithelial cells to induce sheet formation. Cadherin and catenin proteins comprise the adherens intercellular junction while intracellular actin cytoskeletal elements connect neighboring adherens cell junctions providing tension holding the epithelial sheet together.

The carefully coordinated multistep process of epithelial morphogenesis contributes to the shape and function of organs and body parts [1]. Examples of epithelial morphogenesis include embryonic epithelial invagination in the sea urchin, urethral tube development, and prostate epithelial morphogenesis in humans [2-4]. Specific signals trigger morphogenetic events and require an accurate coordination of cytoskeletal and adhesive properties. Through this process, the cell responds to changes in the actin cytoskeleton with structural alterations that result in a structural reorganization of the epithelial sheet. Normal development of these tissues is critical for the proper function of necessary organs, whereas abnormal development of epithilia contributes to developmental problems and many diseases [5, 6]. Some diseases caused by abnormal

epithelial development include: polycystic kidney disease, prostate carcinoma, and abnormal tubule formation in the mammalian urethra [3, 7, 8]. Understanding the general mechanisms regulating epithelial morphogenesis is fundamental to the understanding of the role of epithelial development in various diseases.

*Drosophila l*eg imaginal discs are a congruent system in which to study general epithelial morphogenesis. *Drosophila* imaginal primordia give rise to most of the adult epithelial structures including the adult head, thorax and appendages, and external genitalia [9]. Imaginal discs arise as invaginations of embryonic epithelium and grow by mitosis until metamorphosis, at which time, substantial morphological changes occur. During metamorphosis, nearly all the larval tissues are destroyed by apoptosis, while concurrently, adult organs and structures are derived from imaginal primordia and histoblast nests.

Drosophila melanogaster imaginal disc epithelia provide an excellent model to study the cellular, genetic and molecular biology of the morphogenetic changes in epithelial sheets. *Drosophila l*eg development is well characterized at a cell biological level and is highly amenable to genetic analysis. Prior to metamorphosis, leg imaginal discs are flattened sac-like structures composed of a columnar epithelium on one side, graded into a thin sheet called the peripodial epithelium and attached by a stalk to the inner surface of the larval epidermis [9, 10]. Precisely coordinated conformational shape changes within each epithelial cell stimulates the unfolding and evagination of the leg disc to form an elongated structure that eventually comprises the adult leg. Leg imaginal disc morphogenesis is initiated by systemic steroid hormone as well as intracellular RhoA GTPase signaling [11, 12]. Furthermore, constituent genes of the steroid and RhoA signaling pathways genetically interact in the developing leg suggesting an intersection

between a global steroid hormone response and the ubiquitous intracellular RhoA signaling pathway to control epithelial morphogenesis. Consequently, *Drosophila* imaginal discs make useful tools to study the intersection of hormonal and intracellular signaling pathways with respect to regulating epithelial morphogenesis.

Ecdysone and *Drosophila melanogaster* development

All major post-embryonic developmental transitions in *Drosophila* are controlled by systemic pulses of the steroid hormone, 20-hydroxyecdysone (hereafter referred to as ecdysone) [9, 11-14]. The 10 day life cycle of the holometabolous *Drosophila melanogaster* consists of discrete embryonic, larval, pupal and adult stages. The larval period is organized into three instars punctuated by ecdysone-induced molting. At the end of the third and final instar, a major increase in ecdysone titer causes the progression into the prepupal stage where the morphogenetic events associated with metamorphosis begin (Figure 1).

Metamorphosis is divided into two stages: a brief, 12-hour prepupal period and an 84-hour pupal period [9]. The prepupal period begins with pupariation in which the larval cuticle hardens to form the pupal case and imaginal discs undergo morphogenesis. Adult head eversion marks the start of the following 84-hour pupal period during which the adult cuticle is formed and the adult animal ecloses from the pupal case approximately 192 hours after the larva hatches from the egg.

Ecdysone is synthesized in the ring gland of larvae. The ecdysone receptor is a member of the nuclear hormone receptor family and acts as a heterodimer with another member of the same family, ultraspiracle [15]. When bound to ecdysteroids, the heterodimer binds directly to DNA to regulate gene expression and various

developmental processes. A similar mechanism is exemplified in mammals in which estrogen binding to estrogen receptor and estrogen receptor cofactors regulates gene expression and morphogenesis of mammary ductal formation [16, 17].

Ecdysone pulses occurring in the third larval instar and in prepupae are developmentally relevant to this thesis. Unlike earlier larval pulses which regulate molting, late larval and prepupal ecdysone pulses are associated with many tissue-specific responses including leg disc elongation [9]. The low-titer ecdysone pulse at 12 hours post-second/third instar transition stimulates global regulatory gene networks which control spatial responses in larval tissues and serve to prepare the animal for metamorphosis. Ecdysone pulses at 48/0 hours and 60/12 hours mark the beginning of prepupal and pupal periods respectively triggering cell death in most larval tissues and morphogenesis of adult structures (Figure 1; [13, 14, 18]).

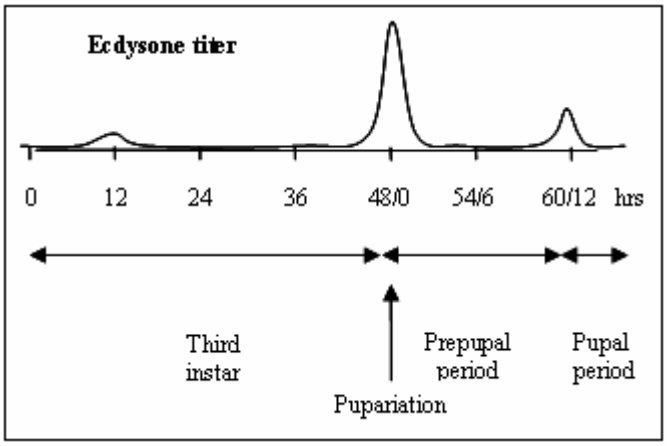

Figure 1: Changes in ecdysone titer at the onset of metamorphosis.

Transient changes in ecdysone titer are indicated. Time 48/0 represents the total time elapsed post 2nd to 3rd instar molt (48 hours) and the beginning of the prepupal stage (0 hours). Ecdysone pulses regulate entry into metamorphosis. The initial stages of leg morphogenesis occur during the first six hours of the prepupal period after pupariation (arrow at 48/0 hours).

Drosophila leg morphogenesis

Major transformations of the folded leg disc to a tubular leg occur during the first six hours of prepupal period, while refinements to the structure of the leg, including segmentation, and the differentiation of hairs and bristles occurs later in the pupal period.

Originally, the imaginal disc cells have an anisometric conformation, with a greater width than length. In the elongated appendage, the cells become isometric, with much of their width diminished (Figure 2A; [19]**)**. The result of this shape change is a lengthening and narrowing of the tubular appendage. Leg disc morphogenesis involves elongation of the disc and eversion to the outside of the animal, collectively referred to as evagination (Figure 2B; [9, 10]). The elongation and unfolding of the leg tissue is driven by the circumferential constriction of the epithelium. Eversion of the appendage to the outside of the larval epidermis then occurs by widening of the stalks and rupturing of the peripodial epithelium [9, 20]. These processes are coordinated by precise cell shape changes caused by the contraction of the apical actin-myosin belt (Figure 2D; [9, 10]). Bundles of actin microfilaments alternating with myosin II proteins form a ring around the apical end of each leg disc epithelial cell (Figure 2C and 2D). The myosin proteins form dimers that, when activated, provide a mechanical force which pulls on the actin filaments and cell-cell adherens junctions leading to apical constriction and morphological cell shape changes.

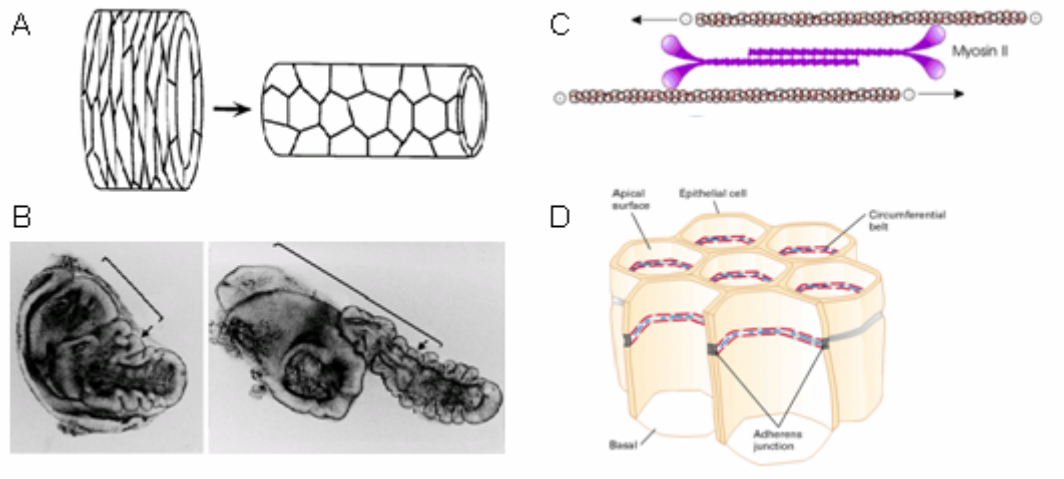

Figure 2: Illustration depicting the cell shape changes during leg elongation.

(A) The originally anisometric cells take on a more isometric shape through the process of epithelial morphogenensis. Six hours after pupariation, imaginal epithelia have become isometric. (B) This reduction in cellular width results in an elongation and narrowing of the tubular structure forming a rudimentary leg. (C) The morphological cell shape changes are driven by actin-myosin contraction. (D)The actin myosin belt connects to neighboring epithelial cells at adherens junctions and provides the force needed for apical circumferential constriction.

Regulation of leg epithelial cell shape changes

A number of genes controlling cell shape changes and presumably actin-myosin contractility are associated with the proper development of the adult leg and wing. Two gene groups influencing leg and wing epithelial morphogenesis include the ecdysone hormone responsive genes and genes that are not directly regulated by ecdysone [11, 12, 21-25]. The Stubble-stubbloid serine protease (Sb-sbd) and broad family of zinc-finger transcription factors are examples of ecdysone hormone responsive genes which play a role in leg and wing development [12, 21, 22, 24, 26]. Additionally, non-hormonal responsive genes including RhoA GTPase and myosin II heavy chain (*zipper*) are necessary for normal leg epithelial morphogenesis [23, 27].

Cell biological analysis has shown that cell shape changes are defective in Sb-sbd and broad mutants [19, 21]. Animals with mutations in *Sb-sbd*, *broad*, *RhoA* and *zipper* exhibit leg and wing malformation phenotypes (Figure 3A and 3B; [12, 23]). This suggests that the malformed phenotype is a good indicator of failure to alter cell shape, an essential part of epithelial morphogenesis. In particular, the leg malformation phenotype is easily scored and characterized by shortened, twisted femurs and bent tibia (Figure 3B). Existing mutations in the genes required for cell shape changes in leg imaginal discs also provide invaluable research tools which can be used to screen for new genetic pathway components (see below).

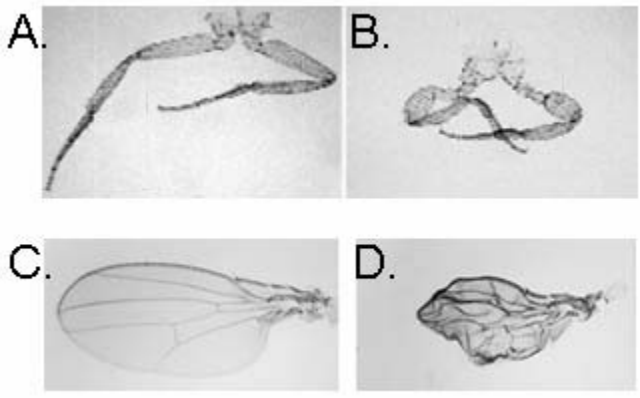

Figure 3: Image depicting the leg and wing wildtype (A and C) and malformed (B and D) phenotypes.

Wildtype legs are pictured in A, while the malformed leg phenotype is represented by short, twisted appendages (B). The wildtype wing is shown in C while the typical crumpled, malformed wing is shown in D [12].

RhoA GTPase signaling in imaginal discs

The Ras superfamily of GTPases are evolutionarily conserved master regulators of various biological processes. These small 20-25 kDa monomeric signaling proteins, numbering over 60 in mammals, fall into five major groups; Ras, Rho, Rab, Arf and Ran.

The Rho family consisting of Cdc42, Rac and Rho, play a special role in regulating the actin cytoskeleton [28-30]. In particular, the *RhoA* (*Rho1*) gene encodes RhoA-GTPase which acts as a molecular switch and activates downstream effector kinases. One role of the effector kinases is the regulation of actin-myosin cytoskeletal contraction and cell shape changes in many tissues including *Drosophila* leg and wing epithelial morphogenesis [31]. In *Drosophila,* RhoA signaling is involved in developmental processes as diverse as head involution, dorsal closure, and imaginal disc morphogenesis [11, 32-34]. Rho proteins are also involved in vertebrate cancers. Studies have shown a positive correlation between Rho protein levels and breast and testicular cancer diagnosis [6, 35, 36]. Furthermore, Rho overexpression leads to the detachment of cells from epithelial sheets in culture [37].

The Rho GTPase protein is active when bound to guanosine triphosphate (GTP) and inactive when GTP is hydrolyzed to guanosine diphosphate (GDP). This activity is modulated by guanine nucleotide exchange factors (GEFs) which activate RhoA by exchanging GDP bound to Rho with GTP. Conversely, GTPase activating proteins (GAPs) negatively regulate GTPases. GAPs operate by catalyzing the intrinsic GTPase activity of Rho GTPases to stimulate the hydrolysis of GTP to GDP (Figure 4). Finally, guanine disassociation inhibitors (GDIs) bind GDP-bound Rho GTPase and hold it in an inactive state away from the membrane, the normal site of Rho GTPase activity [28].

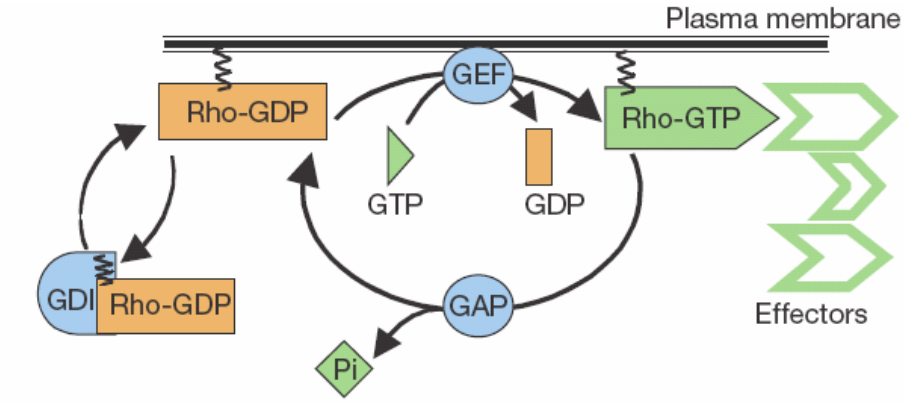

Figure 4: The Rho GTPase cycle. Rho GTPases are regulated by GEFs, GAPs and GDIs. Rho GTPase is activated by the exchange of GDP for GTP by GEFs. Conversely, Rho GTPases are negatively regulated by the catalysis of the hydrolyzing ability of GTPases by GAPs. GDI proteins bind GDP-bound RhoGTPase and retain it in an inactive state [28].

RhoGEF2 activates RhoA GTPase which stimulates downstream effector kinases such as Rho-kinase (Drok) (Figure 5). Rho-kinase phosphorylates myosin light chain kinase and inactivates myosin light chain phosphatase an enzyme which inhibits myosin light chain (Sqh) [38]. Phosphorylation of myosin light chain by myosin light chain kinase and Drok leads to activation of Sqh which in turn activates the myosin II heavy chain (Zipper) [39]. Activation of Zipper creates tension producing activity resulting in the contraction of the actin cytoskeleton. Rho-kinase also activates LIM kinase which phosphorylates and deactivates cofilin. Cofilin is normally dephosporylated and maintained in an activated state by cofilin phosphatase [40]. Thus, the deactivation of cofilin and the activation of myosin II heavy chain allows for F-actin polymerization, cytoskeletal reorganization and contraction. The LIM kinase pathway also results in the nuclear localization of serum response factor and induced transcription (Figure 5).

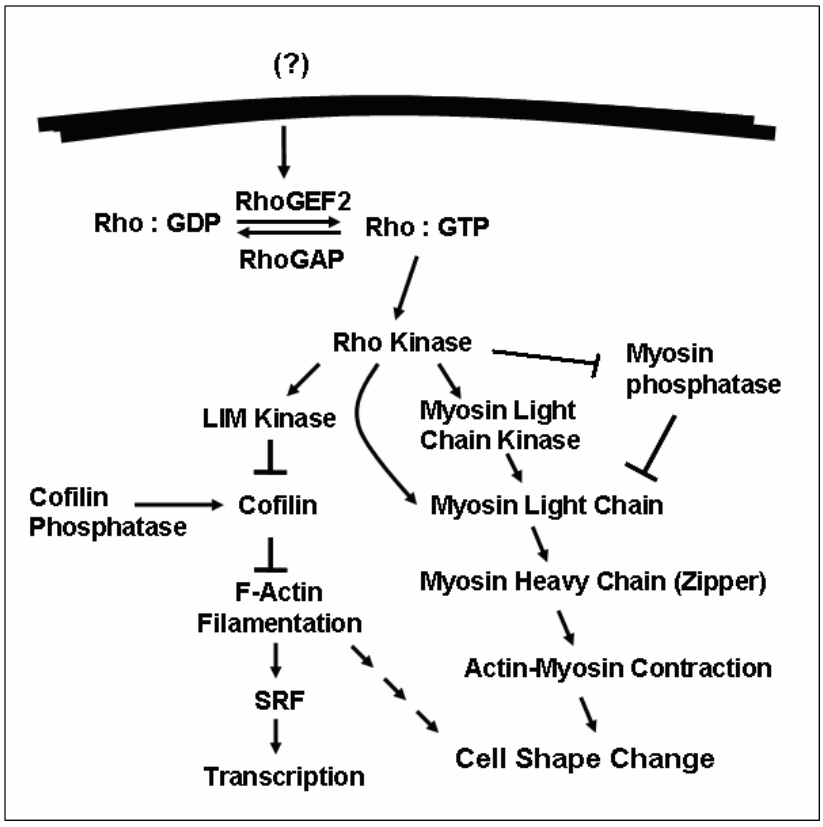

Figure 5: Model of RhoA mediated signaling in imaginal discs.
(see text for discussion).

The downstream activity of the RhoA pathway in the control of cell shape change in leg development is generally understood, however, the initial activation of RhoA signaling as well as the interaction between hormonal and intracellular signals driving leg disc development has not been fully elucidated. Because leg imaginal disc morphogenesis is absolutely dependent upon hormonal signaling at the onset of pupariation and RhoA signaling occurs in most if not all tissues, it has been proposed that ecdysone may temporally regulate RhoA signaling and cell shape changes in developing leg imaginal discs [12]. Other developmental systems also utilize hormonal activation of intracellular signaling pathways. An example is that of mammary development in mammals. In the development of this tissue, estrogen and thryrotropin hormone have each been reported to

activate epidermal growth factor receptor and subsequent downstream effectors via a G-protein-coupled receptor mediated process during ductal morphogenesis in murine mammary tissue [41, 42].

Stubble serine protease and a proposed regulatory model

One possible mechanistic link between the ecdysone hormone response and RhoA signaling is the trypsin-like type II transmembrane serine protease (TTSP) Stubble, encoded by the *Stubble-stubbloid* (*Sb-sbd*) gene. The TTSP family is characterized by a short N-terminal intracellular domain, a transmembrane domain, followed by a variable stem region which includes a cysteine knot in Stubble, and a C-terminal extracellular proteolytic domain (Figure 6; [43]).

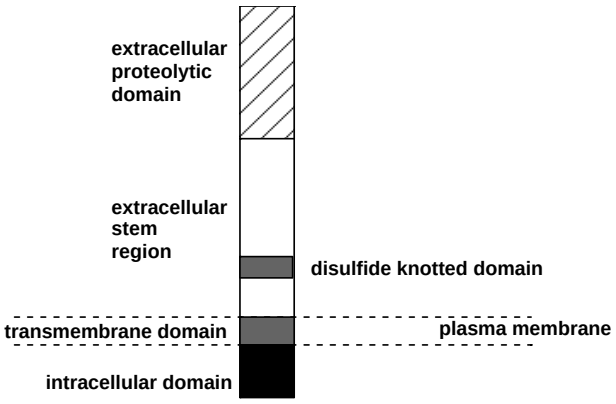

Figure 6: Structure of the *Drosophila* type II transmembrane serine protease. (see text for discussion).

There are currently 15 vertebrate and one *Drosophila* TTSPs described. Many of the vertebrate TTSPs have been associated with various human pathologies including colon and breast cancers, renal carcinomas and ovarian cancer [43]. One TTSP in

humans, the transmembrane protease serine 2 (TMPRSS2) and is regulated by androgenic hormones and has been shown to be proteolytically auto-activated [44]. Although its biological functions have not been determined it has been shown that TMPRSS2 is highly expressed in the epithelium of the human prostate gland and has been implicated in prostate carcinogenesis [45].

The Stubble mutant is characterized by its shortened bristle phenotype later attributed to the disorganization of actin bundling [46]. Mutations in this locus also exhibit leg and wing malformations [12, 19, 22]. Stubble is induced rapidly after exposure to ecdysone and is essential for cell shape changes during leg morphogenesis. *Sb-sbd* mutants interact genetically with several *RhoA* pathway mutants such as *RhoA*, *DRhoGEF2*, *drok*, *zipper*, *myosin phosphatase*, *cofilin phosphatase*, and *blistered/dSRF* to cause malformed legs (Figure 4) and genetic analysis indicates that Stubble acts upstream of RhoA [12].

Based on this evidence, a model has been proposed in which temporally and spatially regulated induction of Stubble by ecdysone results in temporally and spatially restricted activation of RhoA, and reorganization of the actin cytoskeleton leading to leg epithelial morphogenesis (Figure 7; [12]). In this model, two possible mechanisms by which Stubble might activate RhoA are proposed. First, in a mechanism similar to that demonstrated in TMPRSS2 signaling, proteolytic activation of Stubble could lead to the activation of a Rho-guanine exchange factor (RhoGEF) via the Stubble intracellular domain (Figure 7). Second, Stubble might cleave an extracellular molecule such as a membrane associated receptor leading to activation of RhoA. This mechanism has been demonstrated also in TMPRSS2 intracellular signaling via proteolytic activation of the G-protein-coupled receptor PAR2 in the development of the prostate gland [45]. Moreover,

trypsin activates a proteolytically activated receptor (PAR) and Stubble is a member of the trypsin family providing further correlative evidence of the potential for Stubble to play a role in the proteolytic activation of intracellular signaling [47]. An additional mode of regulation of Stubble may be accomplished via serine protease inhibitors (Serpins). Serpins constitute a large family of proteins found in viruses, plants and animals and function as suicide substrate inhibitors which bind serine proteases and are themselves cleaved in the process of inhibiting target serine proteases.

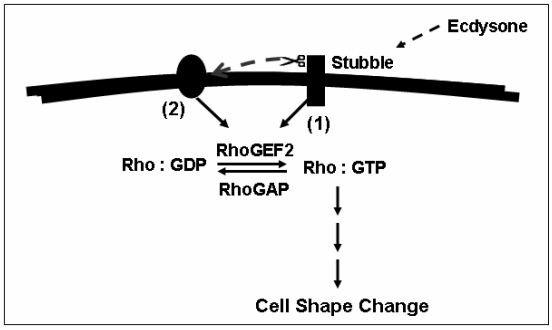

Figure 7: Proposed mechanisms regulating the activation of RhoA in imaginal discs: Stubble, an ecdysone responsive serine protease, activates RhoA via the Stubble intracellular domain (1). Activation of RhoA could also result from Stubble mediated cleavage of an associated membrane bound receptor (2).

Genes involved in leg morphogenesis identified in a genetic screen

In order to better understand the relationship between ecdysone and RhoA signaling during leg development a genetic screen for mutants that interact with *Stubble*, *RhoA*, and *zipper* mutations was conducted (see below). Six mutants were identified, three of which are new alleles of *RhoA*, *DRhoGEF2*, and *zipper*. The remaining three mutations, designated *18-5*, *12-5*, and *31-6*, are all located on the second chromosome and fully complement other mutations in second chromosome genes known to be associated with ecdysone and RhoA signaling [12]. Therefore, they represent potentially

new genes involved in leg epithelial morphogenesis and their characterization may improve our understanding of the mechanisms governing the intersection between ecdysone and RhoA signaling in developing leg epithelia. The *18-5* and *12-5* mutations are pupal lethals while the *31-6* mutation is semi-lethal with death occurring predominantly during pupal development (Callis and von Kalm unpublished data).

As a first step toward identifying the *18-5*, *12-5*, and *31-6* loci, preliminary genetic mapping studies were performed. Preliminary mapping of the *18-5* gene was performed using a combination of classical meiotic and deletion mapping. Both approaches gave consistent results placing the *18-5* gene in the 55D-E cytogenetic region of the second chromosome which provided a starting point for further work to identify the gene. Deletion mapping failed to reveal the chromosomal location of the *12-5* and *31-6* genes. Because the *18-5* and *12-5* mutations exhibit more robust genetic interactions with Stubble and RhoA than *31-6* (Table 1; [12]), and *18-5* is already mapped to a relatively small chromosomal region, *18-5* and *12-5* are the primary foci of this thesis.

Collective preliminary data describing the interactions of the *18-5* mutant strongly indicate a role for the *18-5* gene product in the interaction of the hormone activated Stubble serine protease and the RhoA signaling pathway during leg morphogenesis (Table 3; [12]). Bayer *et al.,* (2003) observed robust genetic interactions between *18-5* and *12-5* with Stubble and members of the RhoA pathway. Therefore, considering the strength of the genetic interactions of the *18-5* and *12-5* mutations with Stubble and members of the RhoA pathway in developing leg imaginal discs; identification and characterization of the genes encoding the *18-5* and *12-5* mutations is likely to better our understanding of the mechanistic relationship between the RhoA pathway and ecdysone hierarchy.

Aims of this thesis

Extensive studies conducted by our lab and others have revealed that ecdysone mediated and RhoA mediated pathways act in a coordinated effort to regulated imaginal disc morphogenesis [11, 12, 48, 49]. The goal of this research is to identify and characterize the *18-5* and *12-5* genes in order to discern the mechanistic relationship between the RhoA pathway and ecdysone hierarchy. The major findings of the work are as follows:

1. I mapped the *18-5* and *12-5* genes to precise molecular locations within the *Drosophila* genome utilizing a P-element recombination mapping technique. This work narrowed the location of the *18-5* locus to within an interval of 112 kb within the *Drosophila* genome sequence. This interval contains 17 known and predicted genes. I also mapped the location of *12-5* to a 2.6 Mb interval of the 2nd chromosome.

2. Based on phenotypic analyses, a candidate gene for the *18-5* mutation was identified. Sequence analysis of the candidate gene in *18-5* homozygotes was inconclusive and requires further analysis.

3. Genetic interaction assays indicate that the *18-5* and *12-5* mutations interact with mutations in *LIM kinase*, *Cdc42*, and *Egfr*.

4. A third site suppression analysis was utilized to try to position *18-5* in the RhoA signaling pathway (Figure 5). Collectively these data place the *18-5* gene product at the level of or upstream of Rho kinase.

MATERIALS AND METHODS

***Drosophila* crosses**

Standard *Drosophila* crosses were conducted as follows unless specifically noted otherwise. *Drosophila* crosses were set up with 4-6 virgin females and 4-5 two-five day old males in individual vials containing standard cornmeal medium. The adult flies were allowed to mate at 25°C for four days, at which time, the adults were transferred to a new vial of medium. The adults were transferred to a third vial on the seventh day following the initial cross resulting in three total vials from which F1 progeny emerged. Upon day ten of the mating cross, the adult flies were anesthetized and placed into a container of mineral oil.

Standard bottle crosses were conducted as follows unless otherwise noted. Flies were set up in crosses of 30 virgin females and 15 two-five day old males in bottles of standard laboratory cornmeal medium. The flies were allowed to mate and lay eggs for four days and subsequently transferred to a fresh bottle. They were again transferred to fresh bottles on day seven and then the animals were euthanized on day ten. The strategy resulted in three bottles which contained F1 progeny of the parental cross.

Deficiency mapping of *18-5* and *12-5*

Deletion mapping was conducted by complementation crosses between *18-5* or *12-5* mutants and flies carrying deletions of the region near 55D-E of the second chromosome. The deficiency mapping was conducted in standard vial crosses. The resultant mutant/deficiency F1 flies were scored for reduced viability relative to sibling classes and leg and wing malformation

Molecular mapping of *18-5* and *12-5*

In order to molecularly map the *18-5* and *12-5* genes, a P-element recombination mapping technique was utilized [50]. Briefly, this method entails determining the recombination distance between a mutation and P-element insertions to the left and right of a mutation. All P-element insertions used have been molecularly mapped to the *Drosophila* genome sequence. This technique permits the calculation of a nucleotide position between the P-elements corresponding to the location of the desired gene on the Drosophila genome sequence.

Molecular mapping of the *18-5* mutation:

The P-element recombination mapping technique entails three total crosses (Figure 8). First, the P_1 cross was performed to obtain the necessary females carrying the P-element and desired mutation in a trans-heterozygous condition (i.e. P, +/+, *18-5*). The P_1 cross was conducted in a standard bottle cross.

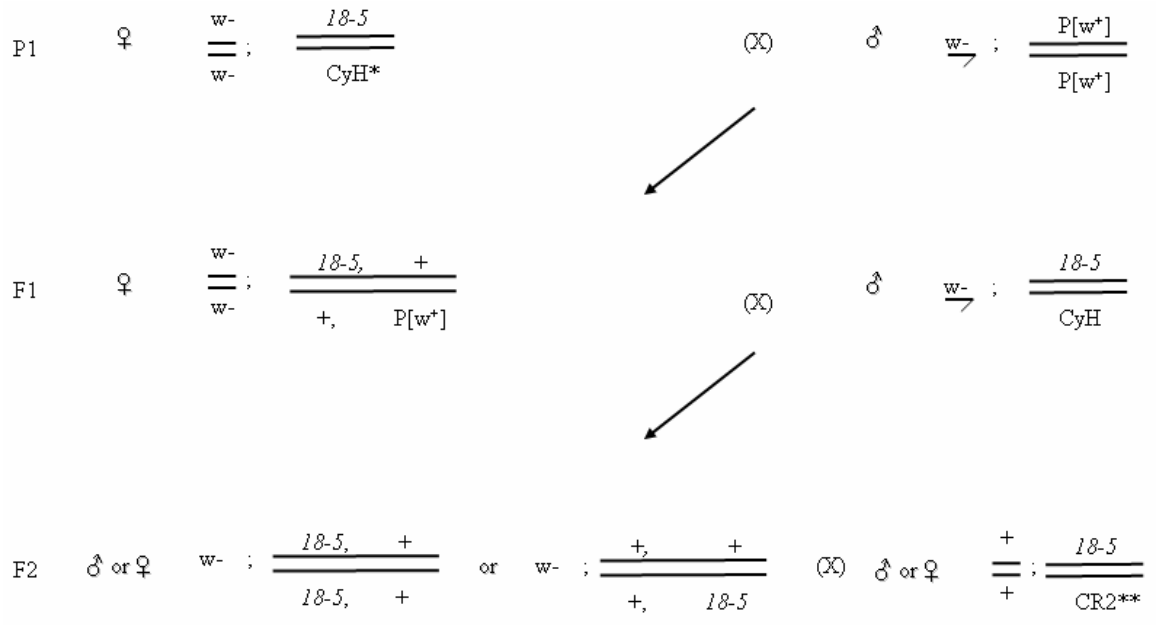

Figure 8: This schematic explains the crossing scheme used to conduct the P-element recombination mapping.

The mapping scheme was adopted for both *18-5* and 12-5 mapping and is shown for the *18-5* mutation. The females carrying both the mutation and the P-element are generated in the first cross. Following recombination in the F1 females, recombinants were distinguished from non-recombinants in the F2 cross (see text for discussion). *CyH is a 2nd chromosomal balancer carrying aGMR-*Hepsin* transgene. Hepsin is a vertebrate type II transmembrane serine protease and GMR is an eye specific promoter [60]. **CR2 is a 2nd chromosomal balancer which carries a sev-*Ras* transgene. Ras is a GTPase and sevenless is an eye specific promoter.

Recombination occurs in the F1 females which were crossed to *18-5/*Curly:Hepsin (CyH) males. The F1 cross was done in a set of 100 separate standard vial crosses, but altered by using 10 virgin females to increase the density of the offspring. An additional change to the standard crossing scheme included culturing F1 animals for 4 days at 25°C and then transfer to 18°C so that all white eyed F2 females could be recovered and crossed as virgins in the third recombination mapping cross.

Approximately 95% of *18-5* homozygotes are either unable to eclose or exhibit severe wing and leg malformation. However, up to 5% of *18-5* homozygotes “escapers” do not exhibit any malformation phenotype and appear to be wildtype. This is significant

in that phenotypically wildtype *18-5, +/+, 18-5* non-recombinants would be scored as recombinants, thus influencing the molecular mapping calculations. In order to distinguish the true recombinant +, +/+, *18-5* animals from the non-recombinant escapers, we tested all F2 white eyed flies to determine if they were recombinants (Figure 9).

All F2 generation white eyed flies were collected as virgins and mated individually to 4-5 virgin female or two to five day old male *18-5*/CR2 animals. In this cross, the homozygous *18-5* escapers produced either animals carrying the CR2 balancer or *18-5* homozygotes (Figure 9). However, if the white eyed fly is a recombinant (i.e. +/*18-5*), then the resultant progeny contains an additional class of *18-5* heterozygotes which appear wildtype. This provides a ratio from which we can determine which animals are true recombinants. The non-recombinant progeny result in a ratio of approximately two curly wing/rough eyed animals to zero wildtype animals. Conversely, the F2 recombinants crossed to *18-5/*CR2 produce a ratio of approximately two curly wing/rough eyed progeny to one wildtype class (Figure 9). A set of stringent criteria were designed for the analysis of F2 crosses in which the results were ambiguous.

1. In order for the F2 progeny to be scored, the CR2 class must have more than 20 animals. If the CR2 class contains less than 20 animals, the data is excluded from the final calculations.
2. In order for the F2 animal to be deemed a non-recombinant, the CR2/WT ratio must be >4.00 and malformation frequency must be >30% unless the number of animals with wildtype eyes is < or = 3.00 or the CR2/WT ratio > 5.00. However, for CR2/WT ratios that are between 3.00 and 4.00, the total malformation must be >50%

3. To be classified as a recombinant: CR2/WT must be <4.00 and mlf must be <50%

In this manner, I was able to determine which F2 white eyed fly was a recombinant due to the much greater number of observed wildtype progeny arising from the F2 recombinant compared to those resulting from the non-recombinant cross.

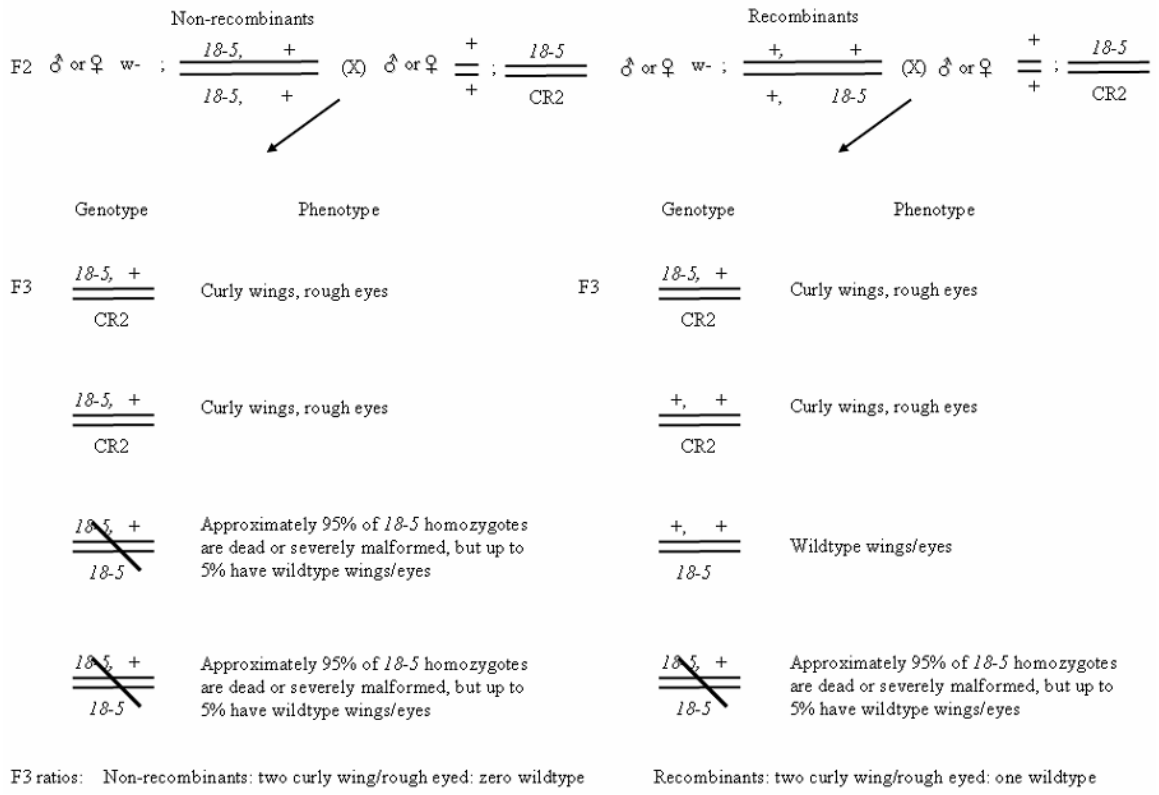

Figure 9: Strategy for distinguishing white eye F2 non-recombinants from the F2 recombinants.

Molecular mapping of the 12-5 mutation

Molecular mapping of *12-5* was conducted using the P-element recombination technique described above, but with key modifications to the strategy. First, the crosses were conducted entirely in bottles of 30 virgin females and 10-15 two-five day old males and the work was performed entirely at 25°C. Second, because the distances between the P-elements and *12-5* were for the most part very large, and because the frequency of *12-5*

homozygote escapers is very low, all F2 white eyed animals were considered to be recombinants. Initial mapping experiments were conducted utilizing a 2nd chromosome rough mapping P-element mapping kit. The P-element mapping kit is a set of molecularly defined P-elements specified by the Bellen lab at the University of Baylor and is available from the Bloomington stock center at the University of Indiana. The insertions are located at regular intervals along the 2nd and 3rd chromosomes and can be utilized for P-element recombination mapping [50].

***18-5* suppression analysis**

Suppression of the *18-5* malformation phenotype was analyzed as described in Figure 10. The frequency of leg and wing malformations and ectopic crossveins was compared in *RhoA*, *18-5*, *Mbs* or *ssh* and *RhoA*, *18-5*, TM2 triple mutants. These crosses were set up in sets of 5 vials of 6 virgin female *18-5*/CyO,GFP; +/+ and 4-6 two-five day old males carrying either *Mbs3* or *ssh*. The flies were allowed to breed and lay eggs on standard cornmeal medium for four days at 25°C. The adults were transferred to new vials in order to continue egg laying on the 4th and 7th day post-P_1 cross. This crossing strategy provided a total of 15 vials per cross. The adults were then euthanized on day ten.

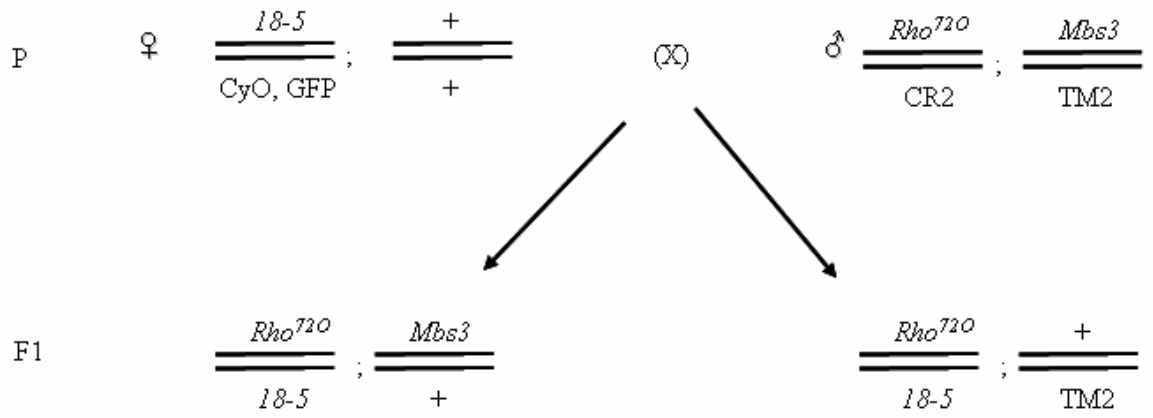

Figure 10: Representative schematic of the suppression analysis crosses.

Image depicts a cross for *18-5* in which the triple mutant for *RhoA*, *18-5* and *Mbs* are scored and compared to the *Rho/18-5* mutant lacking the *Mbs* mutation. Similar experiments were also conducted for *ssh.* Only two of the possible F1 progeny classes are shown.

Sequencing of *DRal GEFmeso*

Extraction of genomic DNA: The *18-5* mutation was rebalanced over CyO carrying an enhanced yellow fluorescent protein (EYFP). This EYFP is under the control of the *Deformed* promoter. Under these conditions, EYFP is strongly expressed in the mouthparts and spiracles of *Drosophila* larvae.

Two sets of 20 wandering 3rd instar *18-5* or *12-5* (as progenitor controls) homozygous larvae were collected based on the lack of EYFP expression. The larvae were placed into 1.5 mL microcentrifuge tubes, snap frozen in liquid nitrogen and stored at -80°C. The larvae were homogenized with a motorized pestle in 250 uL of homogenizing buffer (100 mM Tris-Cl pH 9.1, 50 mM EDTA, 100 mM NaCl, 200 mM sucrose and 0.5% SDS). After the larvae were completely homogenized, 250 uL of phenol and 250 uL chloroform were added and the mixture was spun at 14,000 rpm for 5

minutes at 4°C in an Eppendorf microfuge. The aqueous phase was placed into a new 1.5 mL centrifuge tube and the step was repeated.

Next, the addition of 500 uL of cold 100% ethanol precipitated the DNA and centrifugation pelleted the sample. The pelleted DNA was precipitated again with 500 uL of cold 100% ethanol and pelleted at 14,000 rpm for 5 minutes. Finally, the pellet was washed with 70% ethanol. The pellet was dried in a vacuum centrifuge and resuspended in 25 ul TE +RNase (0.5ul of 100mg/ml RNase to 25 mL TE).

PCR amplification of *GEFmeso*: *GEFmeso* was PCR amplified from *18-5* and *12-5* homozygotes with the use of 12 sets of primers to amplify separate small overlapping amplifications of approximately 500-700 base pairs in length including the entire coding region (Table 2).

Table 1: Primers used for the PCR amplification of *GEFmeso*.

Primer Name	Sequence	Fragment size
Exon1 Forward	CATGTAGACTTTAGATAACAGCGCTG	741
Exon1 Reverse	CCATGTGGATTACGCTGATCCC	
Exon2 Forward	GTTGTCATCGCTGTAAATGGCCG	662
Exon2 Reverse	CATGTGCCCTACAAATTCTCACCG	
Exon3 Forward	TTCGGGCGAGTAGACTAGGG	611
Exon3 Reverse	CACAAGACGATGCCCAAAAGATAGCC	
Exon4 Forward	TTCCGTCTCGTGATCTGGGC	765
Exon4 Reverse	CTGCCGGAGGAGTGAGATACGC	
Exon5 Forward	TCTTCGCTCCCTCCTTCACTGC	560
Exon5 Reverse	TGCTAGCTTTAATTGGCCTTCTAACACG	
Exon6 Forward	CCGCATGTGCATAACTGTTAGGC	675
Exon6 Reverse	GCCAGGTAAGTGTGGGAGC	
Exon7 Forward	ATGATCAGCATGGTGGCGAATAGC	451
Exon7 Reverse	CACACGTACTCTCTGCTTGCCTCC	
Exon8 Forward	CACCCAGAATACTAACTAGGTCAGG	675
Exon8 Reverse	GAAAGTCTGGACAGGCTCACCG	
Exon9 Forward	CTCTCCGCCAGACTTTCTACGC	705
Exon9 Reverse	GAACAAATCGGTACCAGGCACTCC	
Exon10 Forward	ATGCTCTGCTGTGAATCGTACCG	617
Exon10 Reverse	ATGACCAGTCTGCTAGCTACACG	
Exon11 Forward	TCAACTGAGCGCCATCCG	620
Exon11 Reverse	ATCAACATTGCAGCACCTCGGTCG	
Exon12 Forward	CGTGAGATGTCGCAGTGGGAGC	562
Exon12 Reverse	GACTGATGGCCACGTTCTGACTGGG	

Amplification of two large introns was omitted; however, intronic regions close to exons were included to test for possible splice site mutations. The amplification was run with two thermocycle programs settings. Amplification of eleven of the twelve reactions was conducted with an annealing temperature of 55°C, while an annealing temperature of 56°C was found to be optimal for exon 11 (Table 3).

Table 2: Thermocycler settings for the PCR amplification of *GEFmeso*.

55°C				56°C			
Sample	Step	Temp. (in °C)	Time	Sample	Step	Temp. (in °C)	Time
Exon 1				Exon 11			
Exon 2	Denaturation	95	:30		Denaturation	95	:30
Exon 3	Annealing	55	:30		Annealing	56	:30
Exon 4	Extention	72	:45		Extention	72	:30
Exon 5	Cycle numbers	35x			Cycle numbers	35x	
Exon 6	Final Extention	72	7:00		Final Extention	72	7:00
Exon 7	Stop	4	**		Stop	4	**
Exon 8							
Exon 9							
Exon 10							
Exon 12							

The PCR mixture conditions were constant for all runs (1x buffer, 0.5 uM forward and reverse primers, 0.8 mM dNTPs, 2.0 mM $MgCl_2$ .1 uL/reaction DMSO, 1 U Sigma Taq polymerase and 1uL DNA sample). The PCR products were separated on a 0.8% agarose gel with ethidium bromide (20 ul ethidium bromide to 100 mL agarose gel) for 1.5 hours at 60 volts.

Each gel band containing the desired PCR product was excised from the agarose gel. The agarose gel containing the PCR product was weighed and incubated with three volumes of NaI solution at 50°C for five minutes. Next, 5 uL of Geneclean aqueous silica gel suspension (Qbiogene) was added and the sample was incubated at room temperature for 10 minutes with intermittent mixing. The silica gel/DNA mixture was pelleted by centrifugation for one minute at 14,000 rpm. The pellet was washed with “new wash”

(Tris-amiomethane, Qbiogene) and centrifuged for one minute at high speed. The pellet was washed two additional times and dried in a vacuum centrifuge for 15 minutes. Finally, the pelleted silica gel/DNA mixture was washed in 15 uL of purified water and 10 ul of the purified DNA was transferred to a new 1.5 mL microcentrifuge tube.

Cloning: 3.5 uL of each purified PCR product was transferred into a clean 1.5 mL tube followed by the addition of 1.2 ul of salt solution (1.2 M NaCl, 0.06 M $MgCl_2$) and 4 ng of plasmid vector pCRII-TOPO (Invitrogen). The mixture was incubated at room temperature for five minutes, then 37°C for ten minutes and transferred to ice. Next, 18 ul of Oneshot TOP10 chemically competent *E. coli* (Invitrogen) was added and incubated for ten minutes before heat shock treatment at 42°C for 30 seconds. This was immediately followed by the addition of SOC medium (Invitrogen) and shaken at 250 rpm at 37°C for 70 minutes. The cells were then plated onto kanamycin/Xgal plates (50 ug/mL kanamycin, 60 ug/mL Xgal). The colonies were then grown at 37°C overnight and then placed at 4°C.

Next, white colonies of each plasmid transformation were collected and incubated in LB broth with ampicilin (50 ug/mL) at 37°C at 250 rpm overnight. The cells were pelleted at 14,000 rpm for four minutes and then the plasmid DNA was prepared using a Qiagen Plasmid DNA miniprep kit. Finally, the plasmid DNA was quantified on a Nanodrop spectrophotometer.

Sequencing: Samples were sequenced at the Interdisciplinary Center for Biotechnology Research facility at the University of Florida. Sample aliquots were sequenced with the forward and reverse M13 primers using an automated sequencer (Perkin Elmer/Applied Biosystems).

RESULTS

Preliminary genetic interaction data

Preliminary genetic interaction data conducted by Bayer *et al.*, (2003), indicates a possible role for the *18-5* and *12-5* gene products within the RhoA signaling hierarchy regulating leg development. The *18-5* mutant exhibits moderate (25-49%) leg malformation with *zipper* and *Stubble* (Table 3). It also interacts strongly (>50%) with *RhoA* alleles and *Df(2R)Jp8,* a deficiency that uncovers *RhoA*. Additionally, *18-5* exhibits a moderate interaction with *31-6*, a strong interaction with *12-5*, and is lethal when expressed as a homozygote (Table 3). Similarly, genetic data for *12-5* showed that *12-5* also interacts strongly with *RhoA* and zip^{Ebr} mutants and weakly to moderately with various Stubble alleles (Table 3).

Table 3: *18-5* and *12-5* genetic interactions with ecdysone activated Stubble and members of the RhoA signaling pathway regulating leg morphogenesis.

All animals are doubly heterozygous for the alleles indicated. The numbers shown indicate the percentage of animals with malformed legs with the total number of animals scored shown in parentheses. Reduced viability of *12-5, +/+, 18-5* compared to sibling classes indicated by an * [12].

18-5 and *12-5* genetic interactions

	18-5/+	*12-5/+*
$Sb^{6.3b}$/+	*34 (388)*	*17 (229)*
Sb^{70}/+	*37 (299)*	*39 (257)*
$RhoA^{J3.8}$/+	*81 (193)*	*94 (148)*
$RhoA^{E3.10}$/+	*75 (275)*	*93 (125)*
Df(2R)Jp8/+	*72 (281)*	*78 (209)*
zip^{Ebr}/+	*41 (311)*	*71 (186)*
12-5/+	*89 (85)****	*Lethal*
18-5/+	*Lethal*	*89 (85)*
31-6/+	*35 (249)*	*37 (259)*

Deficiency mapping of *18-5*

Deficiency mapping localizes the *18-5* gene to 55D2-55E2. Previous deficiency mapping placed the *18-5* gene in the 55DE cytogenetic region (Callis and von Kalm, unpublished data). This region is 255 kb and contains 58 known and predicted genes. In order to identify potential *18-5* candidate genes, higher resolution mapping of the *18-5* mutation was conducted.

Deletion mapping, a technique utilizing deficiencies or regions in which the DNA is deleted, was conducted to further refine the region containing the *18-5* gene. This was accomplished by complementation tests between deficiencies and the *18-5* mutation. Those deficiencies which exhibit lethality, reduced viability and/or a high frequency of leg malformation are strong candidates to delete the region in which the *18-5* gene is located. Previous mapping using deficiency, Df(2R)Pu66 narrowed the left boundary to the 55D2 region while the right boundary of Df(2R)Pu66 remained unclear and defined as between 55E1 and 56B2. To better define the cytogenetic region containing the *18-5* locus, three additional deficiencies were used to more precisely define the right boundary of Df(2R)Pu66 (Table 4; Figure 11).

Table 4: This table indicates the results of the complementation tests conducted to more precisely define the right boundary of Df(2R)Pu66.

Those deficiencies that complement are noted by a +, while those that fail to complement are represented by a -. ND = not determined.

Deficiency genotype	Bloomington Stock number	Deleted region	*18-5*	Df(2R)Pu66	Df(2R)PC4
w1118; Df(2R)Exel7158, P+PBac{XP5.WH5}Exel7158/CyO	7895	55E2-55E10	+	+	-
w1118; Df(2R)Exel7157, P+PBac{XP5.RB3}Exel7157/CyO	7894	55E7-55F6	+	+	-
W1118; Df(2R)Exel6067, P{XP-U}Exel6067/CyO	7549	55F8-56A2	+	ND	ND

For simplicity during all further discussion Bloomington stock numbers will be used. Ex7895 overlaps with Df(2R)PC4, but does not overlap with Df(2R)Pu66 (Figure 11). Similarly, Ex7894 deletes a region to the right of the region deleted by Df(2R)Pu66, and overlaps with Df(2R)PC4. Furthermore, the deficiencies in table 4 complement the *18-5* mutation, indicating that the mutation is located outside of the boundaries defined by these deficiencies.

The left boundary of Ex7895 is 55E2 and the right boundary of Df(2R)Pu66 has been previously defined as 55E1-56B2. Therefore, the complementation of Ex7895 and Df(2R)Pu66 defines the right boundary of Df(2R)Pu66 as 55E1-2. Thus, the *18-5* mutation is located between 55D2 and 55E1-2.

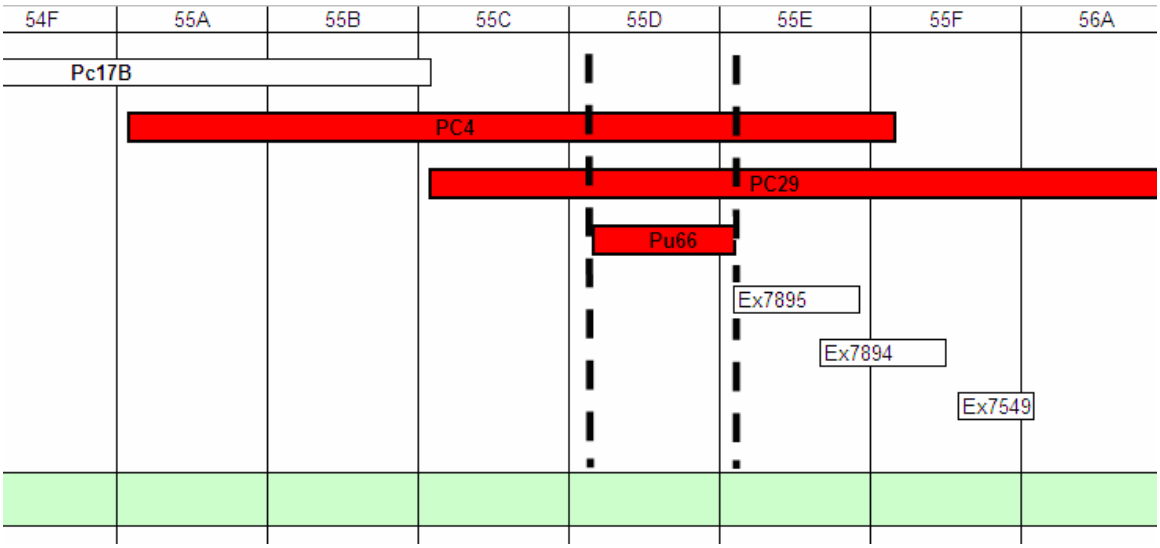

Figure 11: Image depicting the deficiency mapping of *18-5*.

The cytogenetic region is listed above the map. The green bar at the bottom represents the 2nd chromosome. White bars indicate deleted regions that complement *18-5* while those in red do not complement *18-5*.

Many of the breakpoints of *Drosophila* deficiencies are not well defined, so I therefore conducted additional experiments to confirm the left and right breakpoints of Df(2R)Pu66. I used molecularly defined P-element insertions to further map the

deficiency breakpoints. If a lethal molecularly defined P-element insertion is located within the deletion, then the animal carrying both the P-element and deficiency will die, however, if the P-element is outside the deleted region the animal will survive and the molecular position of the P-element will help to define the endpoint of the Pu66 deficiency. Five molecularly defined lethal P-elements were tested (Table 5; Figure 12).

Table 5: Lethal P-element insertions used to better define the breakpoints of the deficiency, Df(2R)Pu66.

The P-element insertions were tested for complementation with deficiency Df(2R)Pu66 and were tested with the much larger deficiency, Df(2R)PC4, to verify the lethality of the P-element insertion. The P-element insertions that complement the deficiencies are represented by +, whereas those that fail to complement are represented by -. (* Semi-lethal P-element insertions in which the complementation data is inconclusive)

Genotype of Stock	Bloomington Stock number	Cytological Location	Df(2R)Pu66/CR2	Df(2R)PC4/CR2
Pbac{w[+mC]=RB}CG5189[e01140]/ CyO	17928	55C9	+	-
P{SUPor-P}CG5226/CyO	13949	55D1	+	-
P{SUPor-P}KG08199/CyO	15126	55E2	+*	+*
P{SUPor-P}KG04591/CyO	14100	55E6	+	-
y1,w67c23; P{lacW}edlK06602/CyO	10633	55E6	+*	+*

I will use a nomenclature describing the cytological location of each P-element for simplification purposes. Transgene insertions P(55C9) and P(55D1) were fully viable over deficiency Df(2R)Pu66 but were lethal over Df(2R)PC4 (Table 5). This indicates that the left boundary of Df(2R)Pu66 must be to the right of 55D1 and indicates that the published cytogenetic boundary of the left side of Df(2R)Pu66 is correct.

P-elements P(55E2) and P(55E6) complemented deficiencies Df(2R)Pu66 and Df(2R)PC4. The molecular position of P(55E2) and P(55E6) are known to be located within the breakpoints of the large deficiency Df(2R)PC4. Therefore, since the P-elements are viable over Df(2R)PC4, this suggests that P(55E2) and P(55E6) are semi-

lethal insertions and the data obtained from the respective crosses with Df(2R)Pu66 are inconclusive. P-element P(55E6) is lethal over Df(2R)PC4, but viable when crossed to deficiency Df(2R)Pu66. The molecular position of P-element 14100 is 55E6. This confirms the deletion mapping conducted with deficiency Ex7895 discussed above in which the right boundary of Df(2R)Pu66 was defined as 55E1-2.

Through this deletion mapping, the region in which the *18-5* locus is located was further refined to a location between 55D2 and 55E2 (Figure 12). This 140 kb region contains a total of 32 known and predicted genes and therefore further mapping was required in order to reduce the number of candidate genes.

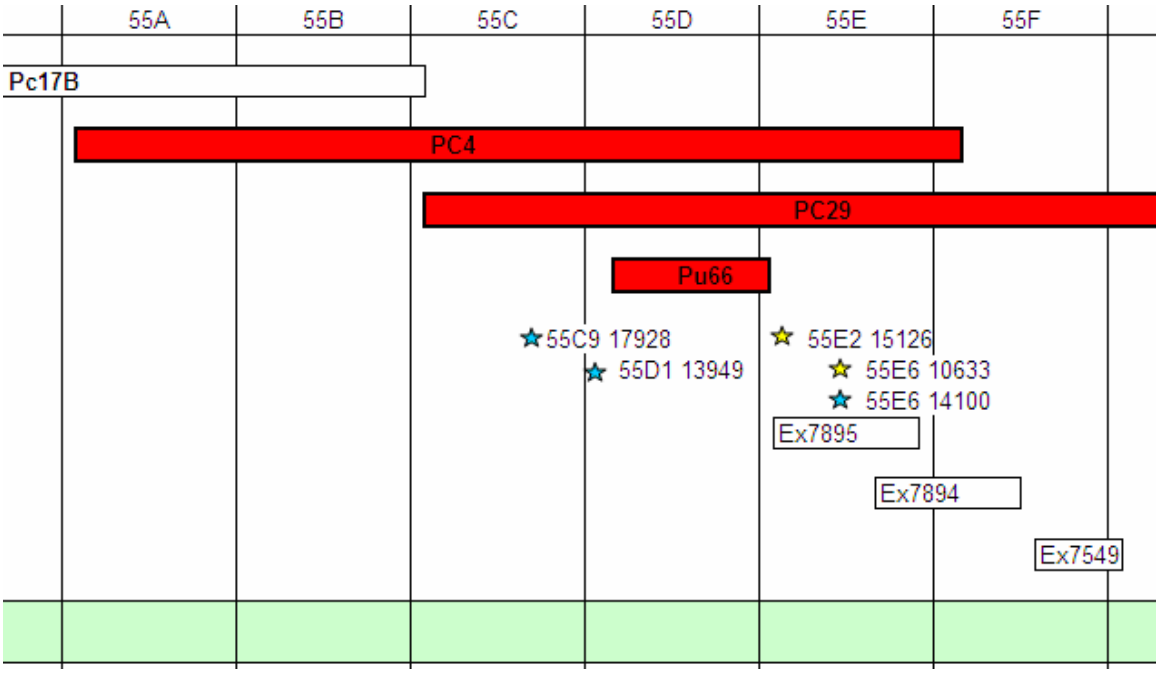

Figure 12: Image depicting the P-element insertions used to further define the boundaries of the deficiency Df(2R)Pu66 used to map *18-5*.

Transgene insertions 17928 and 13949 (blue stars) define the upstream boundary of Df(2R)Pu66 while the lethal insertion, 14100 defines the downstream boundary. The P-elements numbered 15126 and 10633 (yellow stars) are semi-lethal.

Molecular mapping of the *18-5* gene

Molecular mapping defines the location of the *18-5* gene to within a 112 kb interval of the *Drosophila* genome. More precise mapping of the *18-5* gene represents a necessary step toward cloning and gene characterization. To map the *18-5* gene to a more precise location, I utilized a recently published mapping technique that permits molecular mapping of a gene on the published genome sequence [50]. This technique has been shown to be accurate to within 50kb and frequently allows identification of the gene itself. In this approach, mutations are mapped relative to P-element transposons with insertion points that have been molecularly defined in the *Drosophila* genome sequence. To calculate the precise molecular location of the desired gene, the technique utilizes P-element insertions located to the left and right of the gene of interest (Figure 13). Recombination rates between P-elements positioned to the left and right of the desired mutation and the mutation are used to determine a precise molecular position on the genome sequence (Figure 13).

An additional benefit of mapping with P-elements is that several thousand P-element insertions have been mapped to a molecular position in the Drosophila genome. This allows P-elements close to the mutation of interest to be selected which greatly improves the accuracy of the technique.

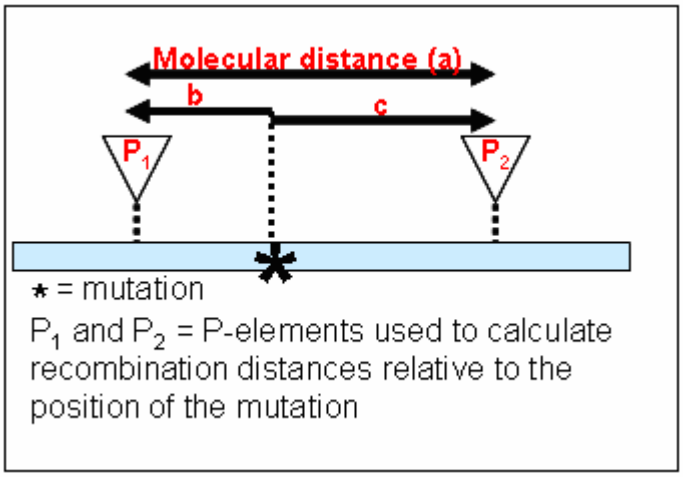

Figure 13: Schematic depicting the P-element recombination mapping technique.

The known molecular distance (a) between two P-elements (triangles) located to the left and right of the mutation (asterisk) is utilized to convert the recombination distances between the P-elements and the mutation into molecular distances between the P-elements and the mutation (b and c). The molecular distances b and c are used to calculate the precise molecular position of the mutation.

The P-element/*18-5* recombination distances were calculated for three P-elements to the left of *18-5* and one P-element to the right of the mutation (Table 6). Two P-element insertions referred to as 12921 and 17538 are located less than 800 kb to the left of the center of Df(2R)Pu66 while 14517 is less than 300 kb to the right of the center of Df(2R)Pu66 (Table 6). P-element 16573 is located a distance of 3,076 kb to the left of the center of Df(2R)Pu66. The recombination rates between the P-element insertions and *18-5* shown in table 6 and Figure 15 have been calculated in centimorgan units. These recombination distances were utilized in the calculation (see below) of the precise molecular position of the *18-5* gene.

Table 6: *18-5/*P-element recombination data used to calculate the molecular position of the *18-5* locus.

Three P-element insertions are located to the left of Df(2R)Pu66 while one insertion is located to the right of Df(2R)Pu66. The distance from the P-element insertion to the center of Df(2R)Pu66 is indicated in kilobases. The recombination distance (RD) between each insertion and the *18-5* mutaion is calculated in centimorgan units (cM).

P-element genotype	Bloomington stock number	Molecular location	Distance from center of Df(2R)Pu66 (in kb)	*18-5/*P-element recombination distance in centimorgans. (total w- and w+ animals scored)
Left of *18-5*				
w1118; P{EPgy2}EY03741/ CyO, P{sevRas1.V12}FK1	16573	11,027,098	3,076	8.6 (1188)
y1 w67c23; P{SUPor-P}KG00600	12921	13,307,435	798	1.9 (1070)
y1 w67c23; P{EPgy2} olf186-FEY9167 /In(2L)Gla	17538	13,370,071	796	1.8 (1941)
Right of *18-5*				
y1 w67c23; P{SUPor-P}KG07142	14517	14,350,084	297	1.2 (3063)

Calculations: The calculation of the molecular position consists of three general steps. First, the recombination distances (RD) between the P-elements and the mutation of interest must be determined in centimorgan units. Second, the RD is then converted into a projected molecular distance (PMD) measured in base pairs (Figure 14). Third, the PMD is subsequently added to the nucleotide position of the upstream P-element to obtain the projected molecular position (PMP) of the gene.

The molecular distance between two P-elements located to the left and right of *18-5* was calculated and divided by the sum of the recombination distances (in cM units) between each P-element and the mutation. This number (bp/cM) was multiplied by the distance in cM between the upstream P-element (P_1 in figure 13) and *18-5*. This projected molecular distance between P_1 and the mutation (PMD_b) was added to the known molecular position of P_1 to get the projected molecular position (PMP) of *18-5* within the *Drosophila* genome sequence. This procedure was repeated for various P-elements in the mapping of *18-5*.

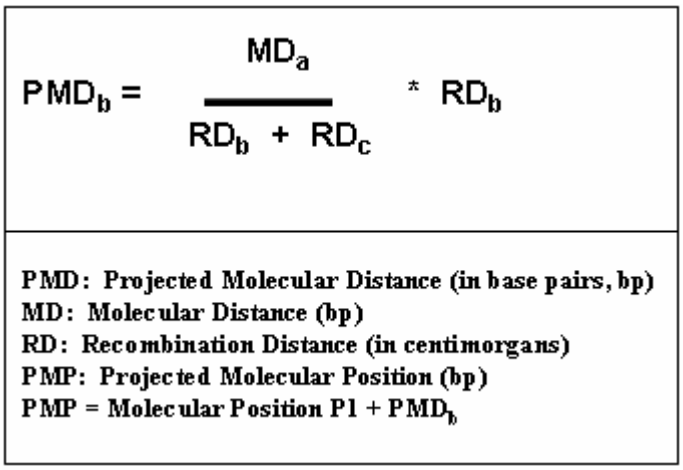

Figure 14: This figure shows the formula used to calculate the projected molecular position (PMP) of the *18-5* mutation.

The projected molecular distance (PMD_b) between the upstream P-element (P_1 from figure 13) and the mutation is calculated by converting the recombination distances (RD b and c from figure 13, measured in centimorgans) of the upstream and downstream P-elements into a molecular distance (PMD) measured in base-pairs. The PMD_b (distance from P_1 to mutation) is added to the nucleotide position of the upstream P-element to identify the precise molecular position of the mutation.

There are two caveats to acknowledge when utilizing this mapping procedure. The mutation must be a lethal mutation (i.e. homozygotes are inviable) and the P-elements must be as close to the unknown locus as possible which improves the resolution of the recombination distances. If the mutation is semi-lethal, the homozygous mutant survivors will appear to be recombinants (see below), thus increasing the recombination frequency between the P-element and the mutation. Unfortunately, *18-5* presents a complicated challenge because up to 5 % of homozygous animals live to adulthood. Therefore, in order to map the *18-5* locus, an additional cross (see methods) was performed to distinguish true F2 generation recombinants from the F2 non-recombinant homozygous adults.

The molecular mapping data for P-elements 16573, 12921, 17538, and 14517 placed the *18-5* locus within a 37 kb region of the genomic sequence located

approximately 75 kb to the left of the left breakpoint of Df(2R)Pu66, the smallest deficiency to uncover *18-5* (Table 6; Figure 15). Given that none of the P-elements tested on the left were closer than 800 kb to the center of Df(2R)Pu66, it is likely that mapping error associated with the distance between the P-elements on the right and Df(2R)Pu66 accounts for the discrepancy in location of the *18-5* locus. However, the mapping data do suggest that *18-5* may be closer to the left end of Df(2R)Pu66.

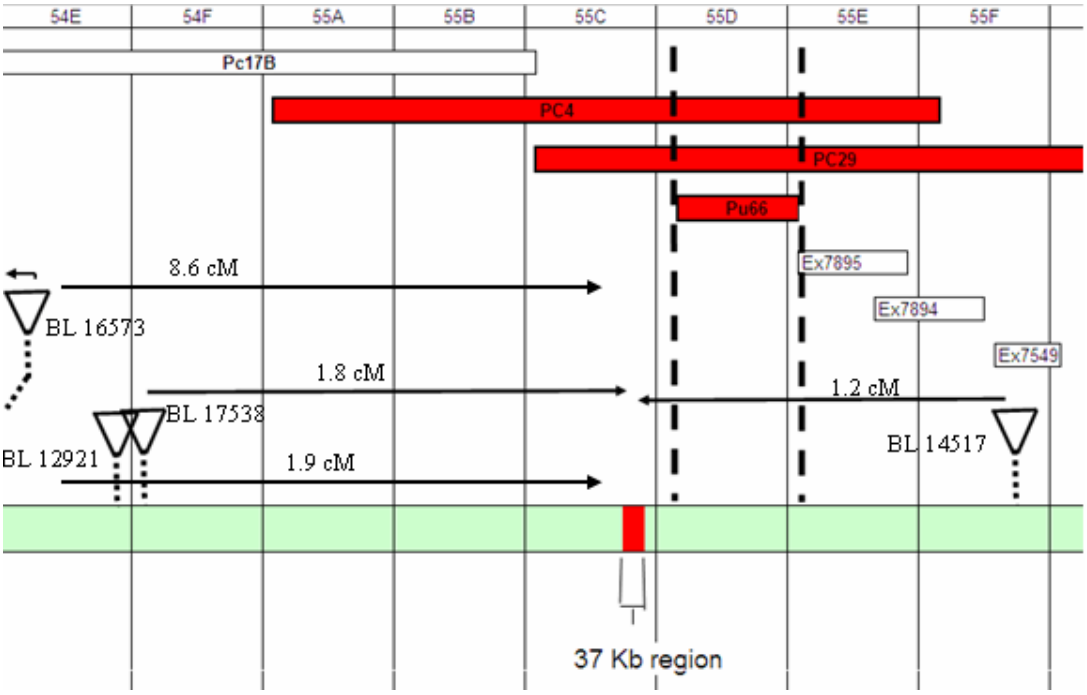

Figure 15: Image depicting the P-elements (triangles with dashes indicating their respective positions) used to map the *18-5* gene and the deficiencies defining the smallest mapped region in which the *18-5* gene is located.

The RD value for each *18-5*/P-element cross is above each arrow (also noted in table 6). The mapping data calculated with the RD values places the *18-5* locus within a 37 kb region of the genome sequence located approximately 75 kb to the left of the left breakpoint of Pu66 (red portion of the chromosome).

A closer view of the mapping region depicted in figure 16 below shows the 75 kb difference in the P-element recombination and deletion mapping techniques. Therefore, taken together, the entire region containing the *18-5* locus mapped using the deletion and P-element recombination mapping techniques represents a region of approximately 112

kb. This region contains 17 known or predicted genes as well as possible non-coding RNAs and siRNAs (Figure 16).

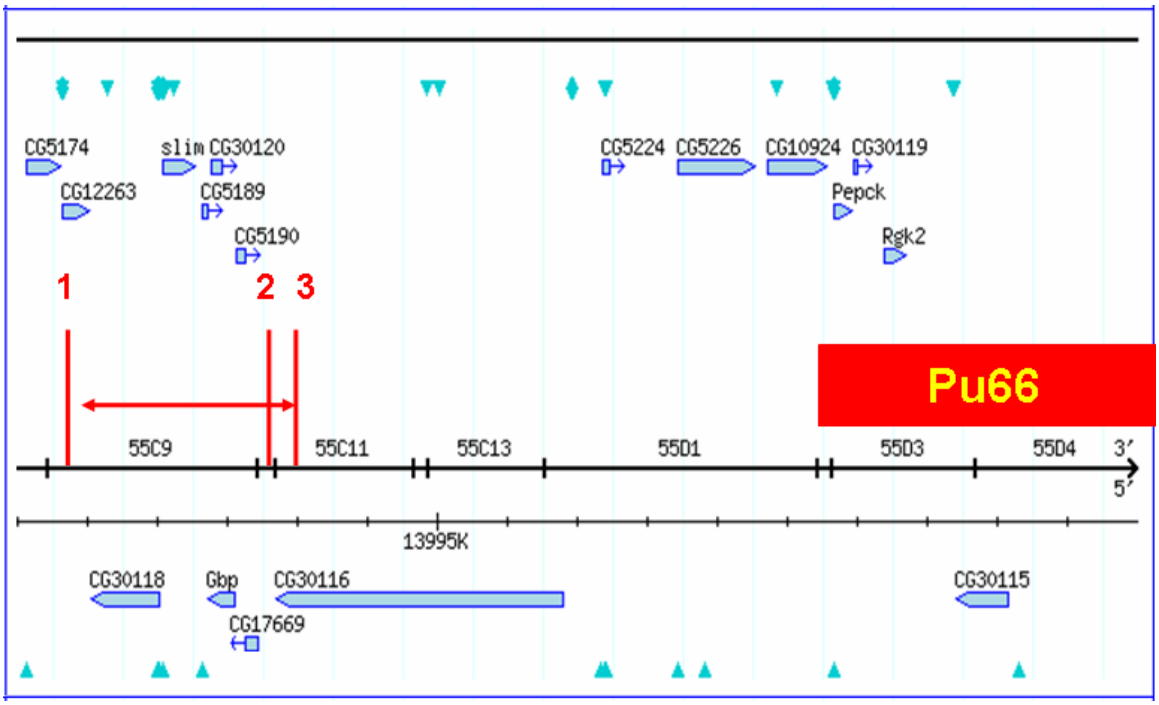

Figure 16: Genomic region in which *18-5* was mapped.

This image shows the three molecular positions of *18-5* mapped by P-element recombination as well as the deficiency Df(2R)Pu66 as a reference. Position 1 was calculated with P-elements 16573 and 14517. Positions 2 and 3 were calculated with 12921 and 14517, and 17538 and 14517 respectively. This image represents the smallest region (approximately 112 kb) in which *18-5* is located. The resulting mapping region contains 17 known or predicted genes (blue bars) as well as many transgene insertions (triangles) useful for complementation testing with *18-5*.

Testing mutations and transgene insertions within the mapped region for complementation with *18-5*

***18-5* complements all mutants and transgene insertions in genes available for testing in the 55D region.** The *18-5* gene was mapped to a region of approximately 112 kb. I expanded this interval to a larger area containing 43 known and predicted genes to be certain not to exclude potential gene candidates. To investigate the possibility that one

of these 43 genes is allelic to the *18-5* mutation, I conducted complementation tests between all available mutant alleles and mobile element insertions in the region (table 7).

I complementation tested transgene insertions in 30 of the known or predicted genes within the region. Those genes which are located in the 112 kb mapped region are listed in bold in table 7. All of the mobile element insertions that were tested with *18-5* were found to complement the mutation (Table 7).

Table 7: Results of complementation tests between *18-5* and various transgene insertions within or close to the 112 kb region containing the *18-5* locus.

Genotype of stock	Gene of interest	Bloomington stock number	Outcome
P{SUPor-P}l(2)55Db$^{425-1}$/CyO	*l(2)55Db*	4563	Complement
b^{1} pr^{1} fs(2)PC4-U^{133} cn^{1}bw^{1}/CyO	*fs(2)PC4-U*	6044	Complement
y^{1} w*; P{lacW}A1-2-54	*EcoI\lacZ$^{A1-2-54}$RA*	10828	Complement
P{PZ}Prp1907838 cn1/CyO; ry506	*Prp19*	12346	Complement
P{PZ}l(2)0877008770 cn1/CyO; ry506	*l(2) 08770*	12357	Complement
w^{1118}; P{GT1}BG02569	***Pepck***	**12815**	**Complement**
y^{1} w^{67c23}; P{SUPor-P}KG01082	*CG30122*	13305	Complement
y^{1} w^{67c23}; P{SUPor-P}KG00319	*CG30332*	13650	Complement
y^{1} w^{67c23}; P{SUPor-P}KG01197	*CG10927*	13706	Complement
y^{1} w^{67c23}; P{SUPor-P}Eip55E^{KG02526}	*Eip55E*	13752	Complement
y^{1} w^{67c23}; P{SUPor-P}KG04893	*CG15092*	13856	Complement
y^{1} w^{67c23}; P{SUPor-P}KG04987	***CG30118***	**13863**	**Complement**
y^{1}; P{SUPor-P}CG5226^{KG03347}/CyO; ry^{506}	*CG5226*	13949	Complement
y^{1} w^{67c23}; P{SUPor-P}CG5224^{KG05424}	*CG5224*	14114	Complement
y^{1} w^{67c23}; P{EPgy2}EY00755a	*CG10924*	15473	Complement
y^{1} w^{67c23}; P{EPgy2}EY06260	*CG5226*	15962	Complement
w^{1118}; P{EP}SP2637^{EP2381}	*SP2637*	17246	Complement
y^{1} w^{67c23}; P{EPgy2}EY07730	***Slim***	**17396**	**Complement**
y^{1} w^{67c23}; P{EPgy2}SP2637^{EY08074}	*SP2637*	17427	Complement
y1 w67c23; P{EPgy2}EY08359	*CG10927*	17454	Complement
y^{1} w^{67c23}; P{EPgy2}EY10175	***CG30116***	**17645**	**Complement**
w^{1118}; PBac{RB}CG33147^{e00779}	*CG33147*	17884	Complement
w^{1118}; PBac{w[+mC]=RB}GstE7[e01100]	*GstE7*	17923	Complement
w^{1118}; PBac{RB}mRpS28^{e02239}/CyO	*MRpS28*	18029	Complement
w^{1118}; PBac{RB}CG10924^{e03788}	***CG10924***	**18191**	**Complement**
w[1118]; PBac{w[+mC]=WH}imd[f02746]	*Imd*	18583	Complement
w^{1118}; PBac{WH}CG18604^{f03280}	*CG18604*	18634	Complement
w^{1118}; P{XP}Atg7^{d06996}/CyO	*Atg7*	19257	Complement
w^{1118}; P{XP}CG33147^{d07752}	*CG33147*	19280	Complement
y^{1} w^{67c23}; P{EPgy2}CG5224^{EY08313}	*CG5225*	19926	Complement

18-5 genetic interactions

***18-5* interacts genetically with 12-5, RhoA, Cdc42, Lim kinase and Egfr, but not with blistered, Ral GTPase, Ral-like protein, Ral guanine nucleotide exchange factor 2, or p21 activated kinase.** *18-5* homozygotes exhibit leg and wing malformation phenotypes characteristic of mutations in genes of the RhoA signaling pathway as well as ecdysone activated *Stubble* mutants (Table 8). *18-5* homozygotes often exhibit the characteristic leg malformations represented by shortened, twisted femurs (67%). The wing of *18-5* homozygotes exhibits 81% overall malformation. The overall wing malformation can be further separated into general wing malformations including crumpled or blistered wings (50%) and wings expressing ectopic crossveins (31%).

Standard vial crosses were conducted in order to better characterize the genetic interactions between mutant alleles of various genes and *18-5* (Table 8). Genetic interactions of *18-5* were analyzed with second-site non-complementation tests between *18-5* and mutations in genes which are proposed to play a role in wing and/or leg development. Briefly, second-site non-complementation is defined as the crossing of two animals with genes at differing loci which results in trans-heterozygote offspring that exhibit the malformed phenotype typically observed in the homozygotes. Moreover, this non-complementation of two genes reflects a functional connection between differing gene products.

The *18-5* ectopic crossvein phenotype is of interest to this study because mutations in genes such as*18-5*, *RhoA*, *Sb*, *Lim kinase*, *Cdc42*, and *Rala* have been shown to exhibit ectopic wing crossveins, thereby suggesting a possible functional relationship between the gene products (Table 8; [48, 51-53]). As heterozygotes, *18-5* mutants do not

exhibit either leg or wing malformation. However, as trans-heterozygotes carrying *18-5,* several genes were shown to interact genetically with *18-5* and exhibit leg and/or wing developmental malformations (Table 8). The genes which interact with *18-5* especially regarding crossvein development include; *LIM kinase* (8%), *RhoA*^{72O} (19%), *Cdc42* (9-53%), and *12-5* (43%) (Table 8), moreover, these mutants do not exhibit ectopic crossveins as heterozygotes.

The ectopic crossvein phenotype is important because it is expressed by mutations in genes such as *RhoA*, *Sb* and *LimK* which play a significant role in the morphogenesis of the leg and wing. The ectopic vein is most often seen between longitudinal veins three and four and between the anterior and posterior crossveins (Figure 17). The ectopic crossvein seen in figure 17 is the additional crossvein most often observed, although, there are often ectopic crossveins in other areas of the wing as well as additional crossveins which remain incomplete and do not reach across the intravein space.

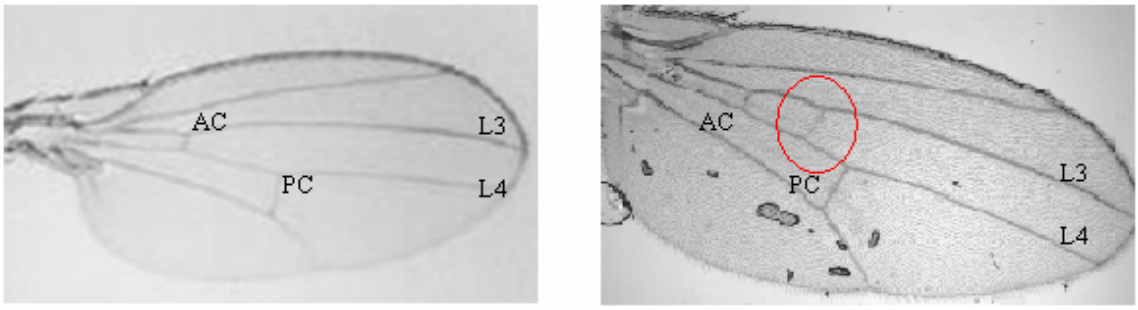

Figure 17: Wing malformation phenotype depicting the extra crossvein.

The photo on the left is of a wildtype wing, note the anterior wing crossvein (AC left, small) and the posterior crossvein (PC right, wider). The image on the right is wing from a +, *Cdc42*^{4}*; +/18-5* animal with an extra crossvein appearing between longitudinal veins three (L3) and four (L4) and between anterior (AC) and posterior (PC) crossveins

Other genes were tested with *18-5* to investigate their prospective roles in wing vein development (Table 8). These include the genes; *blistered* (*bs*), *Rala GTPase* (*Rala*), *Ral-guanine nucleotide exchange factor 2* (*Rgl*), and *Ral-like protein* (*rlip*). Interestingly, none of the trans-heterozygotes carrying one copy of *18-5* and one copy of the indicated allele exhibited any malformation including ectopic wing crossveins (Table 8). Blanke and Jackle (2006) showed that a dominant negative Ral GTPase under the control of an *en*-Gal4 driver resulted in additional but incomplete crossveins [53], but interestingly, the *Rala* mutants I tested with *18-5* did not exhibit any malformations as a trans-heterozygote with *18-5* (Table 8).

Blanke and Jackle (2006) recently showed that RNAi knockdown of *GEFmeso* (a Ral guanine nucleotide exchange factor), resulted in the induction of additional crossveins. Similar ectopic crossveins in the wing are also exhibited in dominant negative and loss of function Cdc42 mutations and Lim kinase mutants [48, 51-53]). Significantly, *GEFmeso* is located within the mapped interval defining the location of the *18-5* gene (*CG30115* in figure 16).

Taken together, this genetic data, along with the location of *GEFmeso* within the mapped interval of *18-5*, makes *GEFmeso* a realistic candidate for the location of the *18-5* mutation locus.

Table 8: Genetic interactions of *18-5*.

All stocks shown were crossed to *18-5/CR2* and the trans-heterozygotes carrying the *18-5* mutation and the mutation in the gene of interest were scored for leg and wing malformation. Numbers indicate the percent malformation observed in the trans-heterozygotes (number in parentheses indicates the total animals and wings scored).

			Malformation		
Genotype of stock or cross	Gene of interest	Leg malformation (total animals scored)	Crumpled wing	Ectopic crossveins	Wing total (total wings scored)
(Oregon R)+/+	Wildtype	0 (71)	0	0	0 (142)
18-5/CR2	18-5	67 (24)	50	31	81 (48)
Df(2R)PC4/CR2	18-5	71 (45)	35	29	64 (90)
w, 12-5/CyH	12-5	17 (106)	46	43	89 (212)
Rho^{72O}/CR2	RhoA	50 (71)	33	19	52 (142)
bw[1] bs[ba]	blistered	0 (97)	0	0	0 (194)
px^{1}, bs^{3}/ px^{1}, bs^{3}	blistered	0 (118)	0	0	0 (236)
y w; P{w[+mC]=lacW}bs [k07909]/CyO	blistered	0 (96)	0	0	0 (192)
y,w{P[Limk1,^{EYO8757}]}	LimK	1 (399)	3	8	11 (798)
Pak6/TM3,Sb1	Pak	0 (44)	0	0	0 (88)
Pak11/TM3,Sb1	Pak	0 (30)	0	0	0 (60)
y^{1}, w*, $Cdc42^{1}$/FM6	Cdc42	0 (44)	0	41	41 (88)
y^{1},w*,$Cdc42^{2}$P{neoFRT}19A	Cdc42	0 (48)	4	9	13 (96)
y^{1},w*,$Cdc42^{3}$/FM6	Cdc42	0 (48)	0	53	53 (96)
y,w,$Cdc42^{4}$P{ry[+t7.2]}/FM6	Cdc42	0 (12)	0	17	17 (24)
w^{67C23} P{lacW}$Rala^{G0501}$/ FM7c	Rala	0 (84)	0	0	0 (168)
w^{67C23} P{lacW}$Rala^{G0174}$/ FM7c	Rala	0 (29)	0	0	0 (58)
w^{67c23} P{lacW}$Rala^{G0373}$/ FM7c	Rala	0 (31)	0	0	0 (62)
P{GT1}$Rgl^{BG02025}$/ TM3,Sb^{1},Ser^{1}	Rgl	0 (48)	0	0	0 (98)
Pbac{Rgl}	Rgl	0 (43)	0	0	0 (86)
w[1118]; PBac{w]}Rlip[c02656]	Rlip	0 (29)	0	0	0 (58)
Df(3r)Exe16272(Rlip)/TM6B	Rlip	2 (55)	0	0	0 (110)
Df(2R)Egfr18, b[1] pr[1] cn[1]/CyO, bw[1]	Egfr	3 (37)	3	0	3 (74)
$Egfr^{t1}$ bw^{1}/CyO	Egfr	0 (30)	0	0	0 (60)
cn[1] Egfr[f2] bw[1] sp[1]/CyO	Egfr	0 (46)	0	0	0 (92)
Egfr[f24]/T(2;3)TSTL, CyO: TM6B, Tb[1]	Egfr	0 (51)	0	0	0 (102)
y w; P{wlacW}Egfr/CyO	Egfr	0 (34)	0	0	0(68)

Sequencing of DRal GEFmeso in *18-5* homozygotes

A candidate gene located within the region in which *18-5* is located is the gene encoding *GEFmeso* (*CG30115* in figure 16). *GEFmeso* encodes a guanine exchange factor which regulates the Ral GTPase and has also been shown to bind the Rho family member Cdc42. Moreover, RNAi experiments targeting *GEFmeso* have been shown to exhibit an ectopic crossvein wing phenotype similar to that of *18-5* [53].

GEFmeso is a guanine nucleotide exchange factor identified as a Ral GTPase activator. The protein has two isoforms, GEFmeso (1237 amino acids) and GEFmeso-short (731 amino acids) (Figure 18, [53]). The GEFmeso-short lacks the Dbl-homology (DH) and Pleckstrin homology (PH) domains found in GEFmeso. The DH domain is responsible for the catalytic activity driving the GDT-GTP exchange within GTPases, while the PH domain binds lipids and is necessary for membrane localization to occur. GEFmeso also contains a Ral GTPase binding region (RBR) and other protein domains including putative PEST and PDZ motifs as well as several proline rich regions. The PDZ domain is most likely required for protein-protein interactions [54].

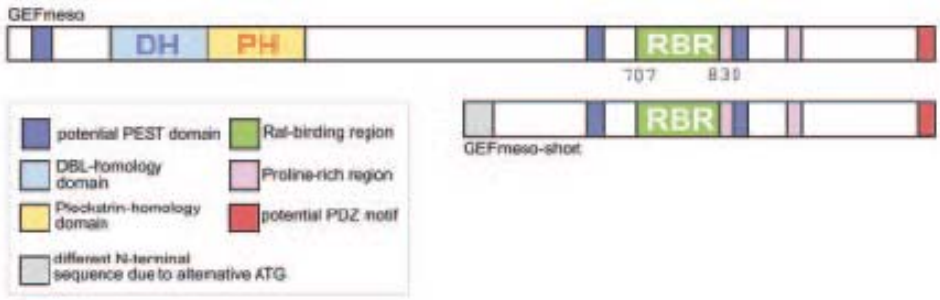

Figure 18: Schematic of GEFmeso structure [53]

To investigate the possibility that *GEFmeso* is *18-5*; I cloned and sequenced *GEFmeso* from *18-5* and *12-5* (as a progenitor control) homozygotes. To accomplish this, I used 24 forward and reverse primers to PCR amplify the coding region of the gene (Table 2). The primers amplified the coding region in 500-700 bp fragments and all primers overlapped by an average of 150 bp for complete coverage. Two large introns between primers 5 and 6 and between 8 and 9 were omitted (Figure 19), but the PCR amplification extended into the intron to include possible splice site mutations.

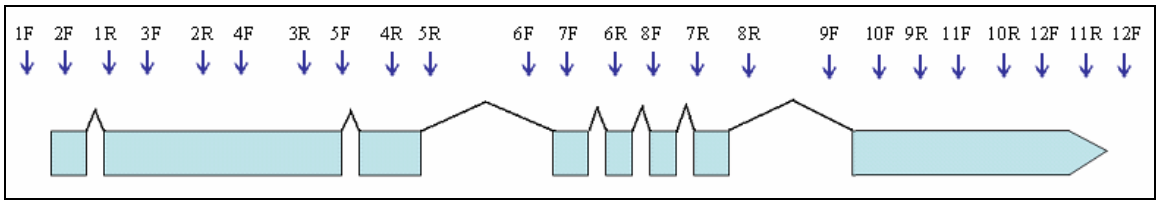

Figure 19: Locations of primers used for the PCR amplification of GEFmeso.

The number indicates the primer used (Table 2) and the forward and reverse primers are labeled with an F and R respectively. The blue blocks indicate exons while the lines connecting the exons represent introns.

Upon initial sequencing of *18-5*, three mutations were observed in the *GEFmeso* sequence. However, two of the mutations are point mutations which were not observed in the second sequencing of the same region from *18-5* homozygotes, nor were they observed in the sequencing of the *12-5* progenitor line. A third mutation observed was an insertion of three amino acids and was identified in two sequencing attempts of *18-5* as well as in the sequence of *12-5*.

One point mutation identified in the initial sequencing of *GEFmeso* is a change from a cytosine to an adenine. This sequence alteration results in an amino acid substitution from a proline to a threonine. The alteration is located in the amino terminal end of the protein just 26 amino acids from the start of the protein in an unconserved region of the protein. This proline to threonine substitution was observed only in the

initial *18-5* sequencing reaction, and not in the second *18-5* sequencing reaction or the sequencing of *12-5*.

A second mutation is point mutation causing a change from a thymine to a cytosine resulting in a stop codon changing to a codon coding for glutamine. This change is significant because it ultimately results in the addition of 17 amino acids attached to the carboxyl end of the protein which encodes a putative PDZ domain. However, this mutation resulting in stop codon alteration was observed only in the initial sequencing reaction of *18-5*, but not in the additional sequencing reactions nor was the mutation observed in the sequencing of *12-5*.

A third mutation is a nine base-pair insertion located near the carboxyl terminal end of the GEFmeso protein (Figure 20). The nine base-pair insertion results in a three amino acid insertion following a valine at position 1139 of the protein sequence. The three amino acid insertion includes an aspartic acid followed by two proline residues. This insertion is not located within a conserved region, but was observed in four different sequencing reactions of *18-5* and two different reactions from *12-5* (Figure 20). Therefore, the insertion was present within the progenitor line used for the EMS screen or the *18-5* and *12-5* mutations are the same allele of the *GEFmeso* gene.

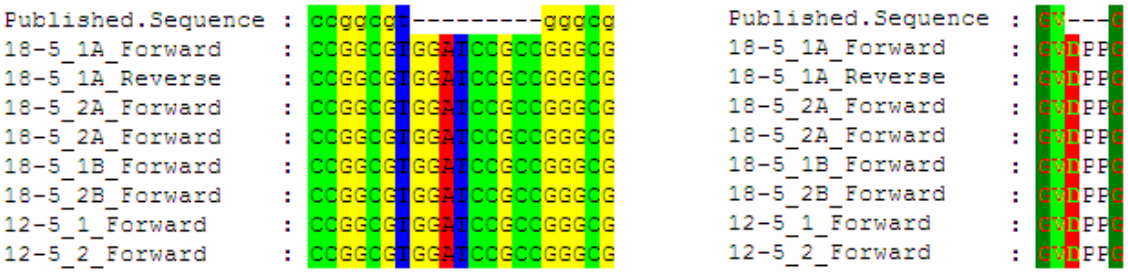

Figure 20: Image showing the nine bp insertion in *GEFmeso* gene sequenced from *18-5* and *12-5* homozygotes (left). This insertion results in a three amino acid insertion of aspartic acid and two proline residues into the GEFmeso protein (right).

Genetic interaction studies place *18-5* at or above Drok in the RhoA pathway

Myosin phosphatase and *slingshot* mutations suppress leg and wing malformation phenotypes exhibited by $RhoA^{72O}$, +/+, *18-5* double heterozygotes.

Genetic interactions between positive regulators of the RhoA pathway typically result in an increased level of leg and wing malformations. Recently, we have discovered (R.Ruggiero, personal communication) that an increase in malformation caused by mutations in two positive regulators of the pathway can be suppressed by the addition of a third site mutation in a negative pathway regulator [55]. This assay offers an excellent opportunity to determine where novel members of the RhoA pathway act within the pathway (see below). In order to determine where the *18-5* locus acts in the RhoA pathway, I utilized a third site suppression analysis.

$RhoA^{72O}$ is a putative null mutation resulting from the imprecise excision of a P-element insertion into the *RhoA* GTPase locus [32]. *18-5* and $RhoA^{72O}$ interact strongly in a heterozygous condition and exhibit wing and leg malformations (Table 8; [12]). Myosin phosphatase negatively regulates nonmuscle myosin II through the dephosphorylation of myosin regulatory light chain (Figure 21; [55]). The myosin binding subunit (MBS) of myosin phosphatase regulates the catalytic subunit of myosin phosphatase in response to upstream signals. A mutated form of *Drosophila* myosin binding subunit (*DMbs3*) is a homozygous lethal EMS mutation. DMbs functions antagonistically to the RhoA signaling pathway and has been shown to suppress malformation of mutations in many RhoA pathway members including zip^{Ebr}, *DRhoGEF2* and $DRhoA^{720}$ [55].

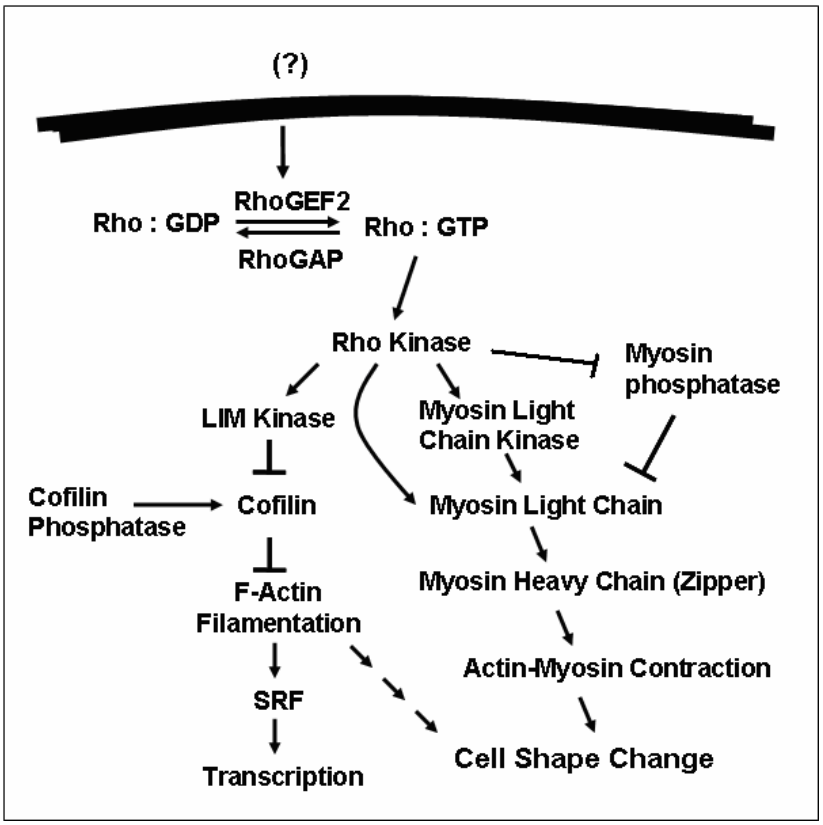

Figure 21: Model of RhoA mediated signaling in imaginal discs.

Additionally, cofilin phosphatase (ssh) acts antagonistically on the Lim kinase side of the pathway to regulate cofilin phosphorylation, thereby regulating actin filamentation (Figure 21; [40, 56]). *18-5* and $RhoA^{72O}$ trans-heterozygotes normally express 50% leg malformation and 52% total wing malformation. The total wing malformation can be separated into 33% general wing malformation represented by crumpled or blistered wings and 19% exhibiting extra crossveins.

However, when a third mutation such as *ssh* or *Mbs3* is carried by *18-5/*Rho^{72O} trans-heterozygotes, the level of malformation is suppressed (Table 9). For example, the addition of the *ssh* acts to suppress leg and wing malformation normally observed in *18-5/*Rho^{72O} trans-heterozygotes. In *18-5,* Rho^{72O}, and *ssh* triple heterozygotes, the total leg malformation is reduced to 12% while the total wing malformation is reduced to 14%,

approximately a four-fold suppression of each malformation (Table 9). Furthermore, in the *18-5*, *Rho^{72O}*, and *ssh* triple heterozygotes, the percent of wings exhibiting crumpled or blistered wings is reduced to 6% while the percent of animals exhibiting ectopic crossveins is 8% (over 5 and 2-fold suppression respectively).

A similar pattern of suppression is observed when an *Mbs* mutant is used to suppress the malformed phenotype associated with *RhoA^{72O}/18-5* trans-heterozygote animals (Table 9). While the amount of leg malformation is similarly reduced to 12% (4-fold suppression), the total wing malformation only reduced to 26% (2-fold suppression), with 7% (5-fold suppression) exhibiting crumpled or blistered wings and no suppression of the ectopic crossvein phenotype.

Table 9: Suppression analysis of *18-5* malformation by cofilin phosphatase (*ssh*) and the myosin binding subunit of myosin phosphatase (*Mbs^{3}*).

See text for discussion.

Genotype	Malformation type	% Malformation (Total animals scored for leg malformation) (Total number of individual wings scored)
18-5/RhoA72O	Leg	50 (71 total animals scored)
18-5/RhoA72O	Total malformed wing	52 (142 total wings scored)
18-5/RhoA72O	Crumpled wing	33
18-5/RhoA72O	Extra crossveins	19
18-5/RhoA^{72O}; ssh/TM2	Leg	12 (55)
18-5/RhoA^{72O}; ssh/TM2	Total malformed wing	14 (110)
18-5/RhoA^{72O}; ssh/TM2	Crumpled wing	6
18-5/RhoA^{72O}; ssh/TM2	Extra crossveins	8
18-5/RhoA^{72O}; Mbs^{3}/TM2	Leg	12 (39)
18-5/RhoA^{72O}; Mbs^{3}/TM2	Total malformed wing	26 (78)
18-5/RhoA^{72O}; Mbs^{3}/TM2	Crumpled wing	7
18-5/RhoA^{72O}; Mbs^{3}/TM2	Extra crossveins	19

This suppression analysis indicates that the *18-5* gene product is active within the RhoA signaling pathway at a location even with or upstream of *Drosophila* Rho kinase (Drok). Drok is a kinase which represents the branch point within the RhoA signaling hierarchy where the signaling pathway bifurcates and results in the activation of the Lim

kinase and myosin II heavy chain branches of the pathway (Figure 21). Moreover, this analysis indicates that ectopic crossvein formation is regulated by the Lim kinase branch of the pathway, whereas both branches of the RhoA pathway regulate leg malformation and the crumpled wing phenotype.

Deficiency mapping of *12-5*

Deficiencies which interact genetically with RhoA and Stubble fail to uncover the *12-5* gene. An autosomal deletion genetic screen conducted in our laboratory to identify genomic regions that interact with *Stubble* or *RhoA* revealed 15 deficiencies located on the second chromosome which interact with one or the other of these loci (Nine of which have previously been shown to complement the *12-5* mutation; Callis, unpublished data). Because *12-5* also genetically interacts with *Stubble* and *RhoA* mutants [12], I asked whether one of the remaining interacting deficiencies deletes the *12-5* locus. To investigate the possibility that one of these deficiencies does indeed delete the *12-5* gene, I crossed six deficiencies that had not previously been tested with the *12-5* mutation (Table 10). Crosses were subsequently tested with *12-5* in a doubly heterozygous condition (i.e. deficiency/+, *12-5*/+). If the deficiency deletes the *12-5* locus, then the subsequent progeny carrying the deficiency and the *12-5* mutation will exhibit malformation phenotypes and possibly show a reduction in viability similar to a *12-5* homozygote.

Crosses were set up under standard vial crosses conditions and all F1 progeny carrying the deficiency and the *12-5* mutation were scored for malformation and reduced viability.

Table 10: List of deficiencies and their locations which were complementation tested with *12-5*.

Crosses between female *12-5* mutants and male flies carrying deficiencies were set up under standard vial crosses conditions and all F1 progeny carrying the deficiency and the *12-5* mutation were scored for malformation and reduced viability. Two deficiencies, Df(2R)PC4 and Df(2R)Pu66 resulted in reduction in viability of the animals carrying *12-5* and the deficiency compared to sibling classes.

Genotype of stock	Bloomington stock number	Deletion breakpoints	Outcome
Df(2L)net-PMF/SM6a	3638	21A1;21B7-8	Complement
Df(2L)BSC16, net^1 cn^1/SM6a	6608	21C3-4;21C6-8	Complement
Df(2L)BSC30/SM6a, bw^{k1}	6999	34A3;34B7-9	Complement
Df(2L)TE35BC-24, b^1 pr^1 pk^1 cn^1 sp^1/CyO	3588	35B4-6;35F1-7	Complement
w^1; Df(2R)Np5, In(2LR)w45-32n, cn^1/CyO	3591	44F10;45D9-E1	Complement
Df(2R)PC4/CyO	1547	55A1; 55F1--2	Malformation/reduced viability
Df(2R)Pu66/CyO	6146	55D2; 55E2	Malformation/reduced viability

Leg and wing malformation phenotypes were observed with two deficiencies on the right arm of the 2nd chromosome. Although not fully lethal, there is a reduction in viability of animals carrying the *12-5* mutation over deficiencies Df(2R)PC4 and Df(2R)Pu66 (Table 11). Notably, *18-5* is nearly fully lethal over Df(2R)PC4 and many of the *18-5*/deficiency animals which survive, exhibit leg and wing malformations.

Table 11: Table showing the viability of trans-heterozygote animals involving *12-5* or *18-5*.

The number represents the percent of the particular trans-heterozygotes which reach adulthood compared to sibling classes (number in parentheses represents the total number of trans-heterozygous animals scored). ND = not determined.

	12-5/+	*18-5*/+
12-5/+	10 (25)	
18-5/+	81 (106)	13 (24)
Df(2R)PC4/+	60 (34)	12 (67)
Df(2R)Pu66/+	71 (44)	ND

Further mapping of the *12-5* locus

P-element recombination mapping indicates that the *12-5* gene is located within the cytogenetic region of 50-56 of the 2nd chromosome. To confirm that the *12-5* locus was indeed located in the 55 cytogenetic region, I conducted P-element recombination mapping as *12-5* mapping as described above. These experiments were performed at low resolution so that the entire second chromosome could be tested. *12-5* mapping was conducted using the Baylor P-element mapping kit available from the Bloomington stock center. The P-element transposons in this collection are spaced at regular distances along the second chromosome (Table 12) and used to calculate the recombination distances between the P-element and the *12-5* mutation.

Table 12: Recombination distances between various P-elements and *12-5*.

P-element	Bloomington stock number	Cytogenetic location	Recombination in cM (total animals scored)
P{SUPor-P}KG00569	13139	21B1	38.7 (486)
P{SUPor-P}KG07698	15116	25A2	42.8 (822)
P{SUPor-P}KG02201	14423	27E6	28.4 (930)
P{SUPor-P}KG07111	14319	30C1	29.7 (814)
P{SUPor-P}porin[KG09266]	16984	32B1	32.4 (830)
P{SUPor-P}KG05572	13901	33A2	31.6 (1588)
P{SUPor-P}CG6116[KG04163]	13360	34B4	32.2 (1247)
P{SUPor-P}KG06763	14241	35B1	32.3 (788)
P{SUPor-P}Tim17b2[KG07430]	14628	35D2	34.1 (1038)
P{SUPor-P}KG08033	14931	36A10	29.9 (835)
P{SUPor-P}KG02815	12989	36E3	28.8 (605)
P{SUPor-P}CG10700[KG04903]	13530	37B13	27.3 (1635)
P{SUPor-P}KG02566	13484	40F1	23.2 (1018)
P{SUPor-P}KG05308	14438	41F3	25.4 (907)
P{SUPor-P}KG01834	14580	43E11	24.3 (577)
P{SUPor-P}CPTI[KG01596]	13731	47A11	26.6 (961)
P{SUPor-P}KG04872	14107	49E1	24.2 (797)
P{SUPor-P}aPKC[KG06602]	**14239**	**51D6**	**15.7 (1358)**
P{SUPor-P}KG07568	**15114**	**53A4**	**15.4 (762)**
y1; P{SUPor-P}KG04591/CyO, ry506	**14100**	**55E6**	**8.6 (961)**
P{SUPor-P}KG07930	**14672**	**55F8**	**13.4 (1411)**
P{SUPor-P}KG06675	14496	59C1	27.3 (932)
P{SUPor-P}KG06046	14470	60F5	34.4 (1405)

The data collected from the crosses between *12-5* and the P-elements indicates that the mutation lies close to the 55E region where the lowest frequency of recombination is observed (Table 12; Figure 22). A 1 cM recombination distance between mutations within the center of the 2nd chromosome equates to approximately a 350-400 kb distance within the genome sequence. Although the resolution of this initial P-element recombination mapping is inadequate for the precise location of the *12-5* locus this data indicates that the *12-5* mutation is located in an interval of approximately 2.6 Mb near the 55E cytogenetic location (Figure 22). Further molecular mapping is required to identify the precise locus of the *12-5* mutation.

Location	21	25	27	30	32	33	34	35	35	36	36	37	40		41	43	47	49	51	53	55	55	59	60
cM	39	43	28	30	32	32	32	32	34	30	29	27	23		25	24	27	24	16	15	8	13	27	34

Figure 22: Schematic of the second chromosome and the P-elements used to map *12-5.*

The schematic represents the P-elements located along the 2nd chromosome. The boxes in light blue depict the cytogenetic location of each insertion while the white boxes below indicate the percentage of recombination between each P-element and *12-5.* The dark blue box represents the centromere.

***12-5* genetic interactions**

Similar to the *18-5* mutation, *12-5* interacts genetically with mutations in *RhoA*, *Cdc42*, and *Lim kinase* and exhibits weak interactions with mutations in *Egfr* and *Pak*, but not with *blistered*, *Rgl*, or *Rlip* mutants. I conducted second-site non-complementation tests between *12-5* and mutations in genes listed in table 13 in order to characterize the functional relationship between *12-5* and various mutations that possibly play a role in leg and wing epithelial morphogenesis. Because *12-5* also exhibits ectopic crossvein phenoytpes that are similar to the *18-5* mutant, it was important to investigate possible genetic interactions between *12-5* and many the same mutant alleles tested for

interactions with *18-5* (Table 13). The results show that *12-5* interacts weakly with *Egfr*, *Cdc42*, *Lim kinase,* and *Pak,* but does not exhibit any malformation phenotype with *blistered* (Table 13).

I also investigated the genetic interactions between *12-5* and *18-5* and *12-5* and *RhoA,* in an effort to more thoroughly examining ectopic crossvein expression. I found that *12-5* interacts strongly with both *18-5* and $RhoA^{72O}$ with respect to ectopic crossvein formation. The trans-heterozygote *12-5/18-5* and *12-5/*$RhoA^{72O}$ F1 progeny exhibit ectopic crossvein phenotypes (43% and 16% respectively) as well as leg (17% and 51% respectively) (Table 13).

Finally, I analyzed the *12-5* genetic interactions with two deficiencies located in the 55DE region, Df(2R)Pu66 and Df(2R)PC4. I found that *12-5* interacts strongly with both deficiencies exhibiting severe leg and wing malformations (Table 13). Interestingly, Df(2R)Pu66 and Df(2R)PC4 have been shown to delete the *18-5* locus (Callis and von Kalm, unpublished data and see above) Overall, the genetic interactions are remarkably similar to the genetic interactions observed in the *18-5* mutation.

Table 13: Genetic interactions of the *12-5* mutation.

All stocks shown were crossed to *12-5/CR2* and the trans-heterozygotes carrying the *12-5* mutation and the mutation in the gene of interest were scored for leg and wing malformation. Numbers indicate the percent malformation observed in the trans-heterozygotes (number in parentheses indicates the total animals and wings scored).

			Malformation		
Genotype of Stock/Cross	Gene of Interest	Leg total (total animals scored)	Crumpled wing	Extra crossveins	Wing total (total wings scored)
(Oregon R)+/+	Wildtype	0 (71)	0	0	0 (142)
w, 12-5/CyH	12-5	80 (25)	36	54	90 (50)
18-5/CR2*	*18-5*	17 (106)	46	43	89 (212)
Df(2R)Pu66/CR2*	*18-5*	17 (44)	17	58	75 (88)
Df(2R)PC4/CR2*	*18-5*	49 (34)	36	53	89 (68)
Rho^{72O}/CyO	RhoA	51 (71)	35	16	51 (142)
y,w{P[Limk1,^{EYO8757}]}	LimK	3 (236)	8	17	25 (472)
Pak6/TM3,Sb1	Pak	0 (29)	3	0	3 (58)
Pak11/TM3,Sb1	Pak	0 (28)	0	0	0 (56)
y,w,Cdc42^{4}P{ry[+t7.2]=neoFRT}/FM6	Cdc42	0 (27)	0	17	17 (54)
w^{67C23} P{lacW}Rala^{G0174}/ FM7c	Rala	0 (26)	0	0	0 (52)
w^{67c23} P{lacW}Rala^{G0373}/ FM7c	Rala	0 (17)	0	0	0 (34)
P{GT1}Rgl^{BG02025}/ TM3,Sb^{1},Ser^{1}	Rgl	0 (44)	0	0	0 (88)
Df(2R)Egfr18, b[1] pr, cn,/CyO	Egfr	7 (15)	8	0	8 (30)
$Egfr^{t1}$ bw^{1}/CyO	Egfr	0 (49)	0	0	0 (98)
cn[1] Egfr[f2] bw[1] sp[1]/CyO	Egfr	0 (39)	0	0	0 (78)
Egfr[f24]/T(2;3), CyO: TM6B, Tb[1]	Egfr	0 (29)	0	0	0 (58)
y w; P{lacW}Egfr[k05115]/CyO	Egfr	0 (64)	0	0	0 (128)

DISCUSSION

Understanding the general mechanisms regulating epithelial morphogenesis is fundamental to the understanding the pathology of epithelia. *Drosophila l*eg imaginal discs are an excellent system in which to study the basic principles of epithelial morphogenesis. *Drosophila* imaginal primordia give rise to most of the adult epithelial structures including the adult head, thorax and appendages, and external genitalia. Imaginal discs arise as invaginations of embryonic epithelium and grow by mitosis until metamorphosis, at which time substantial morphological changes occur. In leg imaginal discs, these morphological changes are coordinated by precise cell shape changes [9, 10, 19]. These cell shape changes act to guide the morphogenesis of many tissues and organs. Specifically, in *Drosophila,* correct epithelial morphogenesis is crucial for the development of legs and wings.

A number of genes controlling cell shape changes and presumably actin-myosin contractility are associated with the proper development of the *Drosophila* adult leg and wing. Two gene groups influencing leg and wing epithelial morphogenesis include the ecdysone hormone responsive genes and genes that are not directly regulated by ecdysone [11, 12, 21-23, 25, 49].

Three studies have provided evidence for ecdysone and RhoA mediated pathways acting in a coordinated effort to regulate imaginal disc epithelial morphogenesis [11, 12, 48]. Consequently, the genes which interact genetically with both the ecdysone and RhoA pathway members are key to deciphering the regulatory mechanism guiding leg and wing epithelial morphogenesis. The *18-5* and *12-5* genes identified by our lab are significant in

that they have been shown to interact with both ecdysone activated Stubble locus as well as RhoA pathway members. The goal of this research is to gain a better understanding of *18-5* and *12-5* in order to help elucidate the mechanism of interaction of steroid hormone and intracellular signaling regulating the process of epithelial morphogenesis.

To identify the *18-5* and *12-5* genes I utilized a P-element recombination mapping technique to identify the precise location of these genes within the *Drosophila* genome [50]. Using this technique I have narrowed the molecular location of the *18-5* locus to an interval of 112 kb within the *Drosophila* genome. This 112 kb region contains 17 known and predicted genes. Additionally, I have also narrowed the location of the *12-5* mutation to a 2.6 Mb interval on the right arm of the 2nd chromosome.

Phenotypic and mapping analysis identified a candidate gene for the *18-5* mutation. This candidate gene was recently identified as a Ral GEF named GEFmeso [53]. Significantly, RNAi experiments targeting GEFmeso identified a mutant ectopic crossvein phenotype which is similar to that observed in *18-5* homozygotes. Moreover, GEFmeso has been shown to bind Cdc42 [53], a gene with which *18-5* interacts (Figure 17). Therefore, I cloned and sequenced GEFmeso from *18-5* and *12-5* (as progenitor controls) homozygotes. The sequencing results were inconclusive and require further analysis.

In order to further characterize the functions of the *18-5* and *12-5* loci, genetic interaction studies were performed. I found that *18-5* and *12-5* genetically interact with mutations in *LIM kinase*, but do not interact genetically with *Pak*, *blistered* (DSRF), or *Ral GTPase.* A gene known to play a role in longitudinal vein formation, *Egfr* [57], exhibited only minor genetic interactions with *18-5* and *12-5.* Furthermore, I have shown that *18-5* and *12-5* interact with *Cdc42* and exhibit ectopic wing crossveins. However,

animals heterozygous for *18-5, 12-5,* or *Cdc42* mutations do not show any leg malformation or crumpled wing phenotypes.

Finally, to better understand the role of *18-5* within the RhoA signaling hierarchy, I have also conducted third site suppression analysis studies. I tested triple mutants carrying *18-5, RhoA*^{720} and *Mbs3* (all in heterozygous condition) as well as *18-5, RhoA*^{720} and *ssh* (also all in heterozygous condition). Myosin phosphatase (Mbs) and Slingshot (ssh) act antagonistically to regulate the RhoA signaling pathway [40, 55, 58]. Interestingly, the addition of third site mutations *Mbs* and *ssh* suppressed the leg and crumpled wing phenotypes normally exhibited in *18-5/RhoA*^{72O} trans-heterozygotes. However, the ectopic crossvein phenotype was only suppressed in combinations carrying a *ssh* mutation. This analysis indicates that with respect to most aspects of leg and wing morphogenesis, *18-5* acts at or above Drok in the RhoA pathway and that crossvein formation is regulated by the Limk/ssh branch of the pathway.

Deficiency and recombination mapping of *18-5*

The P-element recombination mapping of *18-5* considerably narrowed the region in which it is located and as well as the number of possible gene candidates. The 55C9-55D4 region of the 2nd chromosome contains a total of 17 genes. One discrepancy between the recombination and deficiency data is that the recombination data mapped the *18-5* mutation to a region approximately 75 kb upstream from the left breakpoint of the smallest deficiency to uncover *18-5*. This data interpreted literally, suggests that the mutation was mapped with deficiencies to the 55D region as well as further upstream to 55C9-11 by recombination mapping.

The most likely explanation for this discrepancy is that the P-elements used for mapping were not close enough to the *18-5* locus to obtain sufficiently accurate resolution. Zhai et, al. (2003) achieved resolution to within 50 kb in situations where fewer than 10 recombinants per 10000 progeny were observed. In contrast, in my experiments, the lowest number of recombinants was 120 per 10,000 animals. This would presumably result in a decrease in resolution of the mapping recombination rate, thereby decreasing the accuracy of the mapping technique. In view of these limitations, resolution to within 75 kb of the closest deficiency breakpoint seems reasonable.

The resolution could be increased through several methods. We could possibly create a new *18-5* allele with EMS which would exhibit either full lethality or exhibit a stronger mutant phenotype for scoring the escapers. Another option would be to utilize P-elements which are closer to the *18-5* locus. The nearest P-elements used in my experiments were approximately 350 kb away from the projected location of the *18-5* locus. The reason for choosing these P-elements was to ensure that we utilized P-elements located to the left and right of the mutation. Choosing P-elements which are located at a distance of 100-150 kb away from the *18-5* locus would increase the resolution of the molecular mapping. Finally, another method for increasing the resolution would be to increase the number of crosses and animals scored. This would decrease the affect the escapers have on the overall calculations.

To further elucidate the cause of the difference between the molecular mapping and P-element recombination data, I used several lethal insertions to more clearly identify the precise endpoints of the deficiencies. The deficiency Pu66 deletes the genomic region of 55D2-55E4. In an effort to determine if Df(2R)Pu66 actually deletes a portion of the chromosome further to the left of the published breakpoint, I crossed two lethal P-

elements located at 55C9 and 55D1 to the deficiency. The data obtained indicate that the Pu66 deficiency had a left breakpoint which did not extend further upstream than 55D2.

This results in three possible interpretations. First, this indicates that the resolution of the molecular mapping resulted in an incorrect position of the *18-5* mutation and the *18-5* locus is actually located within the region of the deficiency Df(2R)Pu66. A second interpretation is that the molecular mapping correctly positioned the *18-5* locus, but the deficiency deletes a gene which when carried as a trans-heterozygote with *18-5* results in reduced viability and characteristic leg and wing malformations. Finally, the chromosome carrying the deficiency could possibly carry an additional mutation outside of the deleted region which acts similarly to reduce viability and cause the resultant malformation phenotypes. Clearly, further mapping experiments are needed to precisely locate the *18-5* gene. These could include either the P-element recombination mapping with necessary modifications, or possibly using another method such as the male P-element recombination technique [59] which positions a gene to the right or left of a P-element.

***18-5* genetic interactions**

While *18-5* heterozygotes do not exhibit leg or wing malformation, *18-5* homozygous mutants often exhibit the characteristic leg malformations represented by shortened, twisted femurs (67%). Also, *18-5* homozygotes exhibit 81% overall wing malformation, of which, 50% are crumpled or blistered and 31% exhibit ectopic crossveins. *18-5* also interacts genetically with ecdysone activated *Sb* (34-37%) and RhoA pathway members such as *RhoA* (72-81%) and *zipper* (41%) [12]. I have futher identified *18-5* genetic interactions with an additional RhoA pathway member, *Lim*

kinase. 18-5/Lim kinase trans-heterozygotes exhibit a weak genetic interaction exhibiting 11% total wing malformation. Additionally, suppression analysis places the *18-5* gene product within the RhoA signaling pathway at or above Drok (Table 9; Figure 21). This genetic evidence strongly suggests a role for *18-5* in the interaction of ecdysone activated stubble and RhoA regulation of leg and wing morphogenesis.

Of particular interest a malformation phenotype often observed in *18-5* homozygotes is the induction of ectopic crossveins (31%). Significantly, ectopic crossveins have also been exhibited in mutations in *Cdc42, Lim kinase* as well as RNAi experiments targeting *GEFmeso [48, 51-53]*. To investigate the role of *18-5* in the development of wing crossveins, I conducted many crosses specifically analyzing ectopic crossvein expression. I observed ectopic wing crossveins in *18-5/RhoA* (19%) and *18-5/12-5* (43%) trans-heterozygotes. Interestingly, *18-5/Lim kinase* trans-heterozygotes exhibit a weak (8%) genetic interaction regarding ectopic wing crossveins, and *18-5/Cdc42* trans-heterozygotes show weak (9%) to strong (53%) interactions regarding ectopic wing crossveins. Finally, third site suppression analysis indicates that ectopic crossvein formation is regulated by the Lim kinase branch of the pathway (Table 9; Figure 21).

GEFmeso

GEFmeso is a recently identified *Drosophila* Ral guanine exchange factor [53]. It has been shown to bind Cdc42 as well as DRal GTPase. Furthermore, in RNAi experiments targeting *GEFmeso*, investigators found an increase in ectopic crossvein formation. This phenotype has been observed in mutants of several other genes including, *Cdc42, Egfr, RhoA, Sb,* and *Lim kinase* (Table 8; [48, 51-53]. The ectopic crossvein

phenotype has also been observed in *18-5* (31%) and *12-5* (54%) homozygotes. Additionally, the *GEFmeso* gene is located within the Df(2R)Pu66 deficiency. This information suggested that *GEFmeso* was a good candidate to be the *18-5* locus. I tested this hypothesis by sequencing the gene from *18-5* homozygotes. Although the sequencing data for *GEFmeso* were inconclusive, they do not rule out *GEFmeso* as a candidate at this point. The initial sequencing identified three mutations (discussed below). Further analysis is required to fully elucidate potential sequence alterations in the *GEFmeso* gene of *18-5* homozygotes.

Proline to threonine: The initial sequencing of *18-5* identified an amino acid change from a proline to a threonine. Although this amino acid change was not observed in the second sequencing reaction, it remains to be investigated if indeed it is a bona fide alteration to the sequence. This amino acid change could be of importance to the protein because threonine residues are susceptible to phosphorylation which could alter the conformation and hence, the catalytic activity of the protein. Although the putative proline to threonine substitution is not in a highly conserved domain such as the DH, PH or Ral binding region, if phosphorylated, it could potentially disrupt the activity of the protein.

Termination codon alteration: A second mutation found in the initial sequencing, but not observed in the second sequencing of *18-5* is the change of a stop codon to a codon coding for a glutamine. The change of a stop codon to a glutamine results in the lengthening of the protein by 17 amino acids. Recall that the C-terminus of GEFmeso is thought to contain a PDZ domain. The PDZ domain is responsible for protein interactions. An addition to the C-terminus could alter the protein-protein binding of the GEF and interrupt specific localization of the protein needed for correct function.

Insertion: The three amino acid insertion at location 1139 of the 1239 amino acid protein is not located in any region of the protein that is relevant to binding or activation, however, it does occur near a proline rich region and the putative PDZ domain at the carboxyl end of the protein. However, the insertion was also observed in *12-5* homozygotes as well as *18-5* homozygotes, indicating that it existed in the progenitor stock from which the *18-5* and *12-5* mutations were isolated (Figure 20).

Further sequence analysis must be completed before ruling out *GEFmeso* as a candidate for the *18-5* mutation. First, in the unlikely event that the initial sequencing of *18-5* revealed a true mutation, and the second sequencing reactions revealing a wildtype sequence were incorrect, I will sequence the relevant regions a third time to verify the results. Furthermore, I could sequence a third member of the progenitor line, *31-6*, to compare to the initial sequencing of *GEFmeso* in *18-5* mutants. An alternative would be to determine if GEFmeso RNA is altered in quantity or size in the *18-5* mutant. Finally, another approach would be to conduct rescue experiments using genomic fragments from within the 112 kb region.

Possibility that *18-5* and *12-5* are alleles warrants additional analysis

The *12-5* mutation exhibits many similarities to the *18-5* mutation raising the possibility that *12-5* is allelic to *18-5.* Although the possibility is speculative at this time, the evidence supporting the possibility warrants further investigation.

Genetic interactions: *18-5* and *12-5* both interact strongly with *RhoA*, and weakly to moderately with *zip* and *Sb* (Table 1; [12]. Additionally, *18-5* and *12-5* also exhibit similar genetic interactions regarding ectopic crossvein expression with *LIM kinase* (8% and 17% respectively), and both *18-5* and *12-5* each express ectopic

crossveins (17% for both mutations) as trans-heterozygotes with *Cdc42*^{4}. Furthermore, *12-5* and *18-5* mutants both exhibit strong genetic interactions and reduced viability with the deficiency Df(2R)PC4. Altogether, this data raises the possibility that the *12-5* mutation is an allele of *18-5* however, further genetic interaction studies are necessary.

Pupal lethality and reduced viability: The *18-5* and *12-5* mutants both exhibit pupal lethality as homozygotes (Callis and von Kalm, data not shown), and as reported here and by Bayer et, al (2003), the *18-5* +/+ *12-5* double heterozygotes show reduced viability. The reduced viability (only 81% reach adulthood) of the double heterozygotes also is suggestive of lethality during pupal phase development.

Molecular mapping: *18-5* has been narrowed to the interval of 55C9-10-55D4 and preliminary evidence suggests that *12-5* could be mapping to the same locus. Interestingly, the *12-5* mutation was mapped to a cytogenetic region near 55E of the *Drosophila* genome. However, further mapping must be conducted to narrow the *12-5* mapping interval as many genes are located in this region of the *Drosophila* genome including genes encoding RhoA GTPase and Myosin light chain kinase. Altogether, this evidence, although not concrete, is supportive of the possibility that *12-5* and *18-5* are alleles and warrants further analysis.

Broader Significance

Several recent studies have identified an interesting intersection between systemic ecdysone steroid hormone signaling and the cell autonomous intracellular RhoA signaling pathway [11, 12, 25, 27]. Currently there is a major gap in the understanding of how systemic hormone signals regulate intracellular signaling pathways during development. For example, estrogen and progesterone have been shown to play an

important role in the sprouting morphogenesis occurring during alveologenesis in mammary gland development of rats and mice [17]. Estrogen and progesterone activate genes such as IGF-1 and Wnt-4 via a mechanism that is poorly defined. IGF-1 and Wnt-4 are necessary for correct branching morphogenesis of the developing mammary gland, however, the specific pathways activated by these growth factors has not been established [16]. In the developing murine urethra, androgenic hormones regulate *Fgfr,* which is essential for the development of the urethral tube [4]. However the mechanism by which *Fgfr* is activated is again poorly understood, and although *Fgfr* is presumed to activate Receptor Tyrosine Kinase signaling, this has not been demonstrated.

In a vertebrate system somewhat analogous to *Drosophila* leg development, murine prostate gland development has been shown to be regulated by androgenic hormones. Interestingly, studies have shown that during prostate gland development, androgenic hormones regulate the TMPRSS2 type II transmembrane serine protease [44]. Although the function of TMPRSS2 has not been fully elucidated at this time, the TTSP is proteolytically autoactivated in response to androgenic hormones and regulates intracellular signaling via PAR2 [44]. Significantly, TMPRSS2 is highly expressed in prostate as well as colonic cancers indicating that elucidation of the mechanism of hormonally induced intracellular signaling role by TMPRSS2 is a question of considerable clinical significance. In this context it is also clear that understanding the nature of the interaction between ecdysone and intracellular signaling pathways in *Drosophila* imaginal discs is likely to contribute in a fundamental way to a broader understanding of hormonal involvement in vertebrate development and pathology.

Future Directions

Identification of the *18-5* gene product: If it is concluded upon additional *GEFmeso* sequencing, that *GEFmeso* is not *18-5*, then different strategies must be utilized to identify the *18-5* gene. Additional P-element recombination mapping is not an ideal method due to the difficulties in separating white eye recombinants from white eye non-recombinants (see methods). Therefore, alternative approaches must be applied to identify the *18-5* gene. One strategy to consider will be to create designer deletions with hobo elements to better define the region containing the *18-5* gene. Overlapping deletions created by the imprecise excision of hobo elements located less than 200 kb from the *18-5* locus would help determine the precise region in which *18-5* is located. Additionally, presuming that there is a reduction in size or quantity of *18-5* RNA, we could analyze the RNA expression of the genes located in the small region narrowed down by the molecular mapping. We will conduct northern blots of genes of wildtype flies and compare the expression patterns to the same genes from *18-5* homozygotes. Finally another technique is to conduct genomic rescue of the *18-5* malformation phenotype. This technique would allow us to take approximately 10 kb fragments across the 150 kb region and use them for genomic rescue of the mutant phenotype.

Phenotypic characterization of *18-5*: Further characterization of the *18-5* phenotype will improve our understanding of the role of *18-5* in *Drosophila* development. For example, investigations into the role of *18-5* in embryonic, larval and pupal phase development will lead to a better understanding of the spatial and temporal aspects of *18-5* in *Drosophila* development. Additionally, once the gene product is known, we will be able to formulate a hypothesis to test the role of *18-5* in RhoA

signaling, however, experiments to be conducted at this point remain contingent upon the actual *18-5* gene product. Finally, we will conduct experiments to determine whether *18-5* gene is ecdysone responsive.

***18-5* Genetic interactions:** Further experiments are needed to investigate the genetic relationships between *18-5* and other genes with a role in the development of *Drosophila* legs and wings and in particular wing crossvein development. For example, further investigation of possible interactions between *18-5* and *Cdc42*, *Pak,* and *Lim kinase* must be conducted for a better understanding of the respective genetic relationships regarding wing crossvein development. For example, Pak is a downstream effector of Cdc42 and furthermore, Pak has been shown to activate Lim kinase. This represents a possible signaling pathway regulating wing crossvein development. I have shown that *18-5* interacts genetically with *Cdc42* and *Lim kinase* with the respective trans-heterozygotes exhibiting ectopic wing crossveins.

Therefore it is important to further investigate the genetic relationships between *18-5* and *Cdc42, Pak* and *Lim kinase*, because this represents a possible RhoA-Cdc42 connection involving crosstalk between the Cdc42 and RhoA GTPase signaling hierarchies (see figure 21). Interestingly, *Cdc42* does not interact with *RhoA* or other members of the RhoA signaling pathway in leg development. However, *Cdc42* interacts with *Lim kinase* and *18-5* and *RhoA* interacts with *Sb* and *18-5* in wing crossvein development. It remains to be tested whether *RhoA* interacts with other members of the RhoA pathway or *Cdc42* in wing crossvein development. Further experiments investigating this apparent signaling network are needed to fully understand the role of *18-5* in RhoA signaling. Finally, if *GEFmeso* is indeed *18-5*, then this genetic interaction

data should help understand the role of this Guanine nucleotide exchange factor in the developing leg and wing.

***12-5* mapping:** The rough mapping of the *12-5* locus narrowed the region significantly, but further mapping experiments remain necessary to clearly identify the *12-5* gene. This mapping will be conducted using the P-element recombination mapping technique used to map *18-5* (see methods). If the additional P-element recombination mapping fails to identify the *12-5* gene locus, then we will utilize the alternative techniques described for the identification of *18-5* in the case that *GEFmeso* is not *18-5*.

REFERENCES

1. Odell, G.M., Oster, G., Alberch, P., Burnside, B., *The mechanical basis of morphogenesis: Epithelial folding and invagination.* Dev Biol, 1981. **85**(2): p. 446-62.

2. Davidson, L., et al., *How do sea urchins invaginate? Using biomechanics to distinguish between mechanisms of primary invagination.* Development, 1995. **121**: p. 2005-16.

3. Lang, S., et al., *Experimental prostate epithelial morphogenesis in response to stroma and three-dimensional matrigel culture.* Cell Growth and Differentiation, 2001. **12**: p. 631-40.

4. Petiot, A., C. Perriton, and M. Cohn, *Development of the mammalian urethra is controlled by Fgfr2-IIIb.* Dev.and Dis. **132**(10): p. 2441-50.

5. Malliri, A. and J.G. Collard, *Role of Rho-family proteins in cell adhesion and cancer.* Curr Opin Cell Biol, 2003. **15**(5): p. 583-9.

6. Sahai, E. and C.J. Marshall, *Differing modes of tumour cell invasion have distinct requirements for Rho/ROCK signalling and extracellular proteolysis.* Nat Cell Biol, 2003. **5**(8): p. 711-9.

7. Rogers, K.K., et al., *The Rho family of small GTPases is involved in epithelial cystogenesis and tubulogenesis.* Kidney Int., 2003. **63**(5): p. 1632-44.

8. Magee, J., Araki, T., Patil, S., Ehrig, L., Milbrandt, J., *Expression profiling reveals hepsin overexpression in prostate cancer.* Cancer Research, 2001. **61**(15): p. 5692-6.

9. Fristrom, D. and J.W. Fristrom, *The metamorphic development of the adult epidermis*, in *The development of drosophila melanogaster*. 1993, Cold spring Harbor Laboratory Press. p. 843-97.

10. von Kalm, L., D. Fristrom, and J. Fristrom, *The making of a fly leg: a model for epithelial morphogenesis.* Bioessays, 1995. **17**(8): p. 693-702.

11. Ward, R.E., J. Evans, and C.S. Thummel, *Genetic modifier screens in Drosophila demonstrate a role for Rho1 signaling in ecdysone-triggered imaginal disc morphogenesis.* Genetics, 2003. **165**(3): p. 1397-415.

12. Bayer, C.A., et al., *Genetic interactions between the RhoA and Stubble-stubbloid loci suggest a role for a type II transmembrane serine protease in intracellular signaling during Drosophila imaginal disc morphogenesis.* Genetics, 2003. **165**(3): p. 1417-32.

13. Riddiford, L.M., *Hormone receptors and the regulation of insect metamorphosis.* Receptor, 1993. **3**(3): p. 203-9.

14. Thummel, C.S. and J. Chory, *Steroid signaling in plants and insects--common themes, different pathways.* Genes Dev, 2002. **16**(24): p. 3113-29.

15. Thummel, C.S., *Files on steroids--Drosophila metamorphosis and the mechanisms of steroid hormone action.* Trends Genet, 1996. **12**(8): p. 306-10.

16. Visvader, J.E. and G.J. Lindeman, *Transcriptional regulators in mammary gland development and cancer.* Int J Biochem Cell Biol, 2003. **35**: p. 1034-51.

17. Brisken, C., *Hormonal control of alveolar development and its implications for breast carcinogenesis.* J. Mammary Gland Biology, 2002. **7**(1): p. 39-48.

18. Andres, A.J., *Molecular analysis of the initiation of insect metamorphosis: a comparative study of Drosophila ecdysteroid-regulated transcription.* Dev Biol, 1993. **160**(2): p. 388-404.

19. Condic, M.L., D. Fristrom, and J.W. Fristrom, *Apical cell shape changes during Drosophila imaginal leg disc elongation: a novel morphogenetic mechanism.* Development, 1991. **111**(1): p. 23-33.

20. Pastor-Pareja, J.C., et al., *Invasive cell behavior during Drosophila imaginal disc eversion is mediated by the JNK signaling cascade.* Dev Cell, 2004. **7**(3): p. 387-99.

21. Beaton, A.H., et al., *Interaction of the Stubble-stubbloid locus and the Broad-complex of Drosophila melanogaster.* Genetics, 1988. **120**(2): p. 453-64.

22. Appel, L.F., et al., *The Drosophila Stubble-stubbloid gene encodes an apparent transmembrane serine protease required for epithelial morphogenesis.* Proc Natl Acad Sci U S A, 1993. **90**(11): p. 4937-41.

23. Edwards, K.A. and D.P. Kiehart, *Drosophila nonmuscle myosin II has multiple essential roles in imaginal disc and egg chamber morphogenesis.* Development, 1996. **122**(5): p. 1499-511.

24. Gates, J. and C.S. Thummel, *An enhancer trap screen for ecdysone-inducible genes required for Drosophila adult leg morphogenesis.* Genetics, 2000. **156**(4): p. 1765-76.

25. Gotwals, P.J. and J.W. Fristrom, *Three neighboring genes interact with the Broad-Complex and the Stubble-stubbloid locus to affect imaginal disc morphogenesis in Drosophila.* Genetics, 1991. **127**(4): p. 747-59.

26. Kiss, I., Beaton, A. H. Tardiff, J., Fristrom, D. Fristrom, J. W., *Interactions and developmental effects of mutations in the Broad-Complex of Drosophila melanogaster.* Genetics, 1988. **118**(2): p. 247-59.

27. Halsell, S.R., B.I. Chu, and D.P. Kiehart, *Genetic analysis demonstrates a direct link between rho signaling and nonmuscle myosin function during drosophila morphogenesis.* Genetics, 2000. **156**(1): p. 469.

28. Etienne-Manneville, S. and A. Hall, *Rho GTPases in cell biology.* Nature, 2002. **420**(6916): p. 629-35.

29. Hall, A. and C.D. Nobes, *Rho GTPases: molecular switches that control the organization and dynamics of the actin cytoskeleton.* Philos Trans R Soc Lond B Biol Sci, 2000. **355**(1399): p. 965-70.

30. Van Aelst, L. and C. D'Souza-Schorey, *Rho GTPases and signaling networks.* Genes Dev, 1997. **11**(18): p. 2295-322.

31. Van Aelst, L., Symons, M., *Role of Rho family GTPases in epithelial morphogenesis.* Genes Dev, 2002. **16**(9): p. 1032-54.

32. Strutt, D.I., U. Weber, and M. Mlodzik, *The role of RhoA in tissue polarity and Frizzled signalling.* Nature, 1997. **387**(6630): p. 292-5.

33. Magie, C.R., D. Pinto-Santini, and S.M. Parkhurst, *Rho1 interacts with p120ctn and alpha-catenin, and regulates cadherin-based adherens junction components in Drosophila.* Development, 2002. **129**(16): p. 3771-82.

34. Kiehart, D.P., *Wound healing: The power of the purse string.* Curr Biol, 1999. **9**(16): p. R602-5.

35. Lozano, E., M. Betson, and V.M. Braga, *Tumor progression: Small GTPases and loss of cell adhesion.* Bioessays, 2003. **25**: p. 452-63.

36. Sahai, E. and C.J. Marshall, *RHO-GTPases and cancer.* Nat Rev Cancer, 2002. **2**(2): p. 133-42.

37. Vasiliev, J.M., et al., *Rho overexpression leads to mitosis-associated detachment of cells from epithelial sheets: a link to the mechanism of cancer dissemination.* Proc Natl Acad Sci U S A, 2004. **101**(34): p. 12526-30.

38. Amano, M., *Phosphorylation and activation of myosin by Rho-associated kinase (Rho-kinase).* J Biol Chem, 1996. **271**(34): p. 20246-9.

39. Amano, M., *Regulation and functions of Rho-associated kinase.* Exp Cell Res, 2000. **261**(1): p. 44-51.

40. Tanaka, K., Y. Okubo, and H. Abe, *Involvement of slingshot in the Rho-mediated dephosphorylation of ADF/cofilin during Xenopus cleavage.* Zoolog Sci, 2005. **22**(9): p. 971-84.

41. Luo, L., N. Yano, and J.Z. Luo, *The molecular mechanism of EGF receptor activation in pancreatic beta-cells by thyrotropin-releasing hormone.* Am. J. Physiol. Endocrinol. Metab., 2006. **290**(5): p. 889-99.

42. Sukocheva, O., et al., *Estrogen transactivates EGFR via the sphingosine 1-phosphate receptor Edg-3: the role of sphingosine kinase-1.* J Cell Biochem, 2006. **173**(2): p. 301-10.

43. Szabo, R., et al., *Type II transmembrane serine proteases.* Thromb Haemost, 2003. **90**(2): p. 185-93.

44. Kim, T.S., Heinlein, C., Hackman, R., Nelson, P., *Phenotypic analysis of mice lacking the Tmprss2-encoded protease.* Mol Cell, 2006. **26**(3): p. 965-75.

45. Wilson, S., et al., *The membrane-anchored serine protease, TMPRSS2, activates PAR-2 in prostate cancer cells.* Biochem. J., 2005. **388**: p. 967-72.

46. Dobzhansky, T.H., *The manifold effects of the genes stubble and stubbloid in Drosophila melanogaster.* Z. Induct. Abstamm.Vererblehre, 1930. **54**: p. 427-457.

47. Kong, W., McConalogue, K., Khitin, M., Hollenberg, M., Payan, D., Bunnett, N. W., *Luminal trypsin may regulate enterocytes through proteinase-activated receptor-2.* Proc Natl Acad Sci U S A, 1997. **94**(16): p. 8884-9.

48. Chen, G.C., P. Gajowniczek, and J. Settleman, *Rho-LIM kinase signaling regulates ecdysone-induced gene expression and morphogenesis during Drosophila metamorphosis.* Curr Biol, 2004. **14**(4): p. 309-13.

49. Halsell, S.R. and D.P. Kiehart, *Second-site noncomplementation identifies genomic regions required for Drosophila nonmuscle myosin function during morphogenesis.* Genetics, 1998. **148**(4): p. 1845-63.

50. Zhai, R.G., et al., *Mapping Drosophila mutations with molecularly defined P element insertions.* Proc Natl Acad Sci U S A, 2003. **100**(19): p. 10860-5.

51. Baron, M., et al., *Multiple roles of the Dcdc42 GTPase during wing development in Drosophila melanogaster.* Mol Gen Genet, 2000. **264**: p. 98-104.

52. Genova, J.L., et al., *Functional analysis of Cdc42 in actin filament assembly, epithelial morphogenesis, and cell signaling during Drosophila development.* Dev Biol, 2000. **221**: p. 181-94.

53. Blanke, S. and H. Jackle, *Novel guanine nucleotide exchange factor GEFmeso of Drosophila melanogaster interacts with Ral and Rho GTPase Cdc42.* Faseb J, 2005. **20**: p. 683-691.

54. Nourry, C., S. Grant, and J.-P. Borg, *PDZ domain proteins: Plug and Play!* Sci. STKE, 2003. **7**.

55. Mizuno, T., K. Tsutsui, and Y. Nishida, *Drosophila myosin phosphatase and its role in dorsal closure.* Development, 2002. **129**(5): p. 1215-23.

56. Soosairajah, J., et al., *Interplay between components of a novel LIM kinase-slingshot phosphatase complex regulates cofilin.* Embo J, 2005. **24**(3): p. 473-86.

57. Price, J., et al., *Dominant enhancers of Egfr in Drosophila melanogaster: Genetic links between the notch and Egfr signaling pathways.* Genetics, 1997. **147**: p. 1139-53.

58. Sotiropoulos, A., et al., *Signal-regulated activation of serum response factor is mediated by changes in actin dynamics.* Cell, 1999. **98**(2): p. 159-69.

59. Chen, B., et al., *Mapping of Drosophila mutations using site-specific male recombination.* Genetics, 1998. **149**(1): p. 157-63.

60. Leppert, A., *Genetic analysis of RhoA signaling during epithelial morphogenesis in Drosophila.* MS Thesis, University of Central Florida, 2004.